Journal of Systematic Innovation

Journal of Systematic Innovation

Definition of Journal

Scientific Objectives

Support the international scientific community in its written production Science, Technology and Innovation in the Field of Engineering and Technology, in Subdisciplines of electromagnetism, electrical distribution, sources innovation in electrical, engineering signal, amplification electrical, motor design science, materials in electrical power, plants management and distribution of electrical energies.

ECORFAN-Mexico SC is a Scientific and Technological Company in contribution to the Human Resource training focused on the continuity in the critical analysis of International Research and is attached to CONAHCYT-RENIECYT number 1702902, its commitment is to disseminate research and contributions of the International Scientific Community, academic institutions, agencies and entities of the public and private sectors and contribute to the linking of researchers who carry out scientific activities, technological developments and training of specialized human resources with governments, companies and social organizations.

Encourage the interlocution of the International Scientific Community with other Study Centers in Mexico and abroad and promote a wide incorporation of academics, specialists and researchers to the publication in Science Structures of Autonomous Universities - State Public Universities - Federal IES - Polytechnic Universities - Technological Universities - Federal Technological Institutes - Normal Schools - Decentralized Technological Institutes - Intercultural Universities - S & T Councils - CONAHCYT Research Centers.

Scope, Coverage and Audience

Journal of Systematic Innovation is a Journal edited by ECORFAN-Mexico S.C in its Holding with repository in Taiwan, is a scientific publication arbitrated and indexed with semester periods. It supports a wide range of contents that are evaluated by academic peers by the Double-Blind method, around subjects related to the theory and practice of electromagnetism, electrical distribution, sources innovation in electrical, engineering signal, amplification electrical, motor design science, materials in electrical power, plants management and distribution of electrical energies with diverse approaches and perspectives, that contribute to the diffusion of the development of Science Technology and Innovation that allow the arguments related to the decision making and influence in the formulation of international policies in the Field of Engineering and Technology. The editorial horizon of ECORFAN-Mexico® extends beyond the academy and integrates other segments of research and analysis outside the scope, as long as they meet the requirements of rigorous argumentative and scientific, as well as addressing issues of general and current interest of the International Scientific Society.

Editorial Board

Arbitration Committee

Assignment of Rights

The sending of an Article to Journal of Systematic Innovation emanates the commitment of the author not to submit it simultaneously to the consideration of other series publications for it must complement the Originality Format for its Article.

The authors sign the Authorization Format for their Article to be disseminated by means that ECORFAN-Mexico, S.C. In its Holding Taiwan considers pertinent for disclosure and diffusion of its Article its Rights of Work.

Declaration of Authorship

Indicate the Name of Author and Coauthors at most in the participation of the Article and indicate in extensive the Institutional Affiliation indicating the Department.

Identify the Name of Author and Coauthors at most with the CVU Scholarship Number-PNPC or SNI-CONAHCYT- Indicating the Researcher Level and their Google Scholar Profile to verify their Citation Level and H index.

Identify the Name of Author and Coauthors at most in the Science and Technology Profiles widely accepted by the International Scientific Community ORC ID - Researcher ID Thomson - arXiv Author ID - PubMed Author ID - Open ID respectively.

Indicate the contact for correspondence to the Author (Mail and Telephone) and indicate the Researcher who contributes as the first Author of the Article.

Plagiarism Detection

All Articles will be tested by plagiarism software PLAGSCAN if a plagiarism level is detected Positive will not be sent to arbitration and will be rescinded of the reception of the Article notifying the Authors responsible, claiming that academic plagiarism is criminalized in the Penal Code.

Arbitration Process

All Articles will be evaluated by academic peers by the Double Blind method, the Arbitration Approval is a requirement for the Editorial Board to make a final decision that will be final in all cases. MARVID® is a derivative brand of ECORFAN® specialized in providing the expert evaluators all of them with Doctorate degree and distinction of International Researchers in the respective Councils of Science and Technology the counterpart of CONAHCYT for the chapters of America-Europe-Asia- Africa and Oceania. The identification of the authorship should only appear on a first removable page, in order to ensure that the Arbitration process is anonymous and covers the following stages: Identification of the Journal with its author occupation rate - Identification of Authors and Coauthors - Detection of plagiarism PLAGSCAN - Review of Formats of Authorization and Originality-Allocation to the Editorial Board-Allocation of the pair of Expert Arbitrators-Notification of Arbitration -Declaration of observations to the Author-Verification of Article Modified for Editing-Publication.

Instructions for Scientific, Technological and Innovation Publication

Knowledge Area

The works must be unpublished and refer to topics of electromagnetism, electrical distribution, sources innovation in electrical, engineering signal, amplification electrical, motor design science, materials in electrical power, plants management and distribution of electrical energies and other topics related to Engineering and Technology.

Presentation of the content

In the first article we present, *Morphological analysis and its effect on the optical properties of carbon nanospheres as a function of synthesis time* by Ordóñez-Casanova, Elsa Gabriela, Trejo-Mandujano, Héctor Alejandro, Saucedo-Acuña, Rosa Alicia and Villanueva-Montellano, Alfredo, with adscription in Universidad Autónoma de Ciudad Juárez- Instituto de Ingeniería y Tecnología, the next article we present, *Innovative Ti/Fe/Eu-Carbon composite for Cephalexin adsorption* by Gómez-Vilchis, J.C., García-Rosales, G., Lóngoria-Gándara, L.C. and Tenorio-Castilleros, D, with adscription in Tecnológico Nacional de México – Instituto Tecnológico de Toluca, International Atomic Energy Agency and Instituto Nacional de Investigaciones Nucleares, the next article we present, *Electromagnetic theory: Electromagnetic pulse in the laboratory by* Guzmán-Tinajero, Pedro, Hernández-Gómez, Víctor Hugo and Castro-Fuentes, Aide, with adscription in Facultad de Estudios Superiores Cuautitlán UNAM, the last article we present, *Influence of concentration, acid type and calcination temperature on TiO₂ synthesis* by Del Ángel-Sánchez, María Magdalena & Martínez-Carreón, María de Jesús, with adscription in Universidad Tecnológica Gral. Mariano Escobedo and Universidad Autónoma de Nuevo León.

Content

Article	Page

Article

Morphological analysis and its effect on the optical properties of carbon nanospheres as a function of synthesis time

Análisis morfológico y su efecto en las propiedades ópticas de las nanoesferas de carbono en función del tiempo de síntesis

Ordóñez-Casanova, Elsa Gabriela*[a], Trejo-Mandujano, Héctor Alejandro [b], Saucedo-Acuña, Rosa Alicia [c] and Villanueva-Montellano, Alfredo [d]

[a] ROR Universidad Autónoma de Ciudad Juárez- Instituto de Ingeniería y Tecnología • P-4527-2015 • 0000-0002-8970-5730 • 98163

[b] ROR Universidad Autónoma de Ciudad Juárez- Instituto de Ingeniería y Tecnología • F-4342-2019 • 0000-0001-7776-8825 • 94458

[c] ROR Universidad Autónoma de Ciudad Juárez- Instituto de Ciencias Biomédicas • GWM-5880-2022 • 0000-0003-1051-7858 • 121305

[d] ROR Universidad Autónoma de Ciudad Juárez-Instituto de Ingeniería y Tecnología • KPB-0290-2024 • 0000-0002-8864-9984 • 430444

CONAHCYT classification:

Area: Physics-Mathematics and Earth Sciences
Field: Physics
Discipline: Physics of the solid state
Subdiscipline: Optical properties

Abstract

This work presents the effect of synthesis time on morphology and its influence on the optical properties of microwave-assisted carbon nanospheres. To analyze the correlation between the synthesis time and the growth in size of the nanospheres, the morphology of the nanostructures was characterized by scanning electron microscopy (SEM) and X-ray diffraction (XRD). Their optical properties were analyzed by UV-Vis spectrophotometry, and the Tauc method was used to estimate the optical band gap. The results reveal that the time variation in the synthesis does have a significant influence on the size, shape, and amount of sample obtained. The optical properties presented slight modifications. With these results, we can provide an easy reproducibility of simple and inexpensive methods to optimize the growth of carbon-based nanoparticles, which can bring advances in the synthesis of materials and improvements in their optoelectronic applications.

Nanospheres, Morphology, UV-Vis
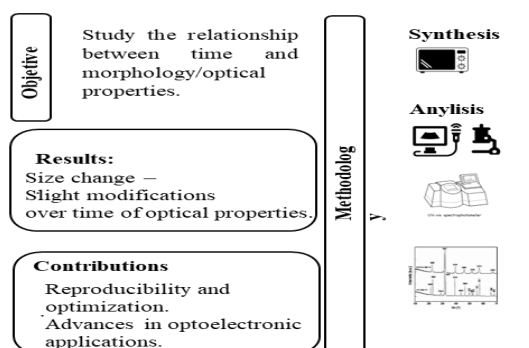
Resumen

El efecto del tiempo de síntesis en la morfología y su influencia en las propiedades ópticas de las nanósferas de carbono asistidas por microondas se presenta en este trabajo. Para analizar la correlación entre el tiempo de síntesis y el crecimiento en tamaño de las nanósferas, se caracterizó la morfología de las nanoestructuras mediante microscopía electrónica de barrido (SEM) y difracción de rayos X (XRD). Sus propiedades ópticas se analizaron mediante espectrofotometría UV-Vis, y se utilizó el método de Tauc para estimar el ancho de banda óptico. Los resultados revelan que la variación del tiempo en la síntesis tiene una influencia significativa en el tamaño, la forma y la cantidad de muestra obtenida. Las propiedades ópticas presentaron ligeras modificaciones. Con estos resultados, podemos proporcionar una fácil reproducibilidad de métodos simples y económicos para optimizar el crecimiento de nanopartículas a base de carbono, lo que puede generar avances en la síntesis de materiales y mejoras en sus aplicaciones optoelectrónicas.

Nanoesferas, Morfologia, UV-Vis

RENIECYT
Registro Nacional de Instituciones y Empresas Científicas y Tecnológicas
I702902 CONAHCYT

Journal of Systematic Innovation

Article

Introduction

The continuous search for simple, inexpensive, and innovative methods to obtain carbon-based nanostructures such as: carbon nanotubes, fullerenes, nanoonions, etc. (Ordoñez et al., 2013, Ordoñez et al 2019), has been a key driver in this research. In addition, carbon nanostructures have great potential in different applications, covering areas such as materials science, biomedicine, and nanotechnology.

In recent years, the alternative use of the microwave oven around materials science has proven to be a valuable tool for reducing synthesis costs (Adeola, et al.,2023).

Microwave-assisted syntheses offer advantages over conventional heating techniques by avoiding temperature gradients and long reaction times. The effectiveness of microwaves in materials synthesis is attributed to the ability of some chemical compounds to absorb energy in the microwave range and convert it into heat, thus accelerating the generated reactions (Pawelski D et al., 2023).

Similarly, the microwave radiation synthesis technique has also become popular because of (Zhou, J., Xu et al.,2020). A pioneering study conducted by the University of Wyoming has demonstrated the effectiveness of this method in converting raw carbon powder into nano graphite, a finding that reinforces the use of microwave technology in the production of C60 and C70 fullerenes (Masi et al. 2021), as well as carbon quantum dots (De Medeiros et al., 2019), demonstrating size variation in allotropic materials.

In recent years, this technique has also been used in a wide range of materials beyond carbon allotropes, encompassing inorganic, organic compounds, and biomaterials (Siebert et al.,2019). Mainly focused on increasing the improvement of the purity and properties of the materials obtained (Kumar, A et al., 2020).

Some materials that present improvements using this technique are nanoparticles of metals such as silver (AgNP), gold and platinum (Dankovich, 2014), allowing a finer control over the size, morphology, and distribution of the nanoparticles. As well as, titanium dioxide (TiO_2), zinc oxide (ZnO) and (Fe+2) (Ashok, 2014. Zhu,2012. Pati ,2014).

Some ceramics improve their density and mechanical properties (Borrel et al., 2013), and in the case of polymers obtaining them can achieve improvements in properties (Kuo,2016).

From these previous investigations, we carried out the preparation of 4 samples with 99% purity grade graphite powder in wafer form, using as a synthesis method a conventional microwave, which emits electromagnetic radiation around 2.45 GHz.

The main approach was to vary only the synthesis time of the samples every 2.5 minutes. The results revealed a diversity of morphologies, but the presence of sphere-like nanostructures stands out.

Corroborating that the synthesis time does affect the morphology and size. With respect to the optical properties, they were analyzed by UV-Vis spectroscopy and using the Tauc method, for the study of the optical forbidden band, it is verified that any change in the surface, size and presence of impurities affects the properties.

Methodology

A conventional microwave oven with electromagnetic radiation around 2.45 GHz at an output power of 1000 W was used. As carbon source, powdered graphite with a purity of 99% was used, using equivalent amounts of 1 milligram per sample placed in a ceramic crucible, completely covered.

Four samples were prepared, varying the synthesis time at intervals of 2.5 minutes each. The initial amount per sample of graphite powder was 1.2 grams. At the end of each synthesis, they were weighed and an average decrease of .2 grams per sample was observed.

Results and discussion

SEM characterization

Figure 1 shows the SEM micrographs of the four samples using scanning electron microscope, (SU5000, Hitachi).
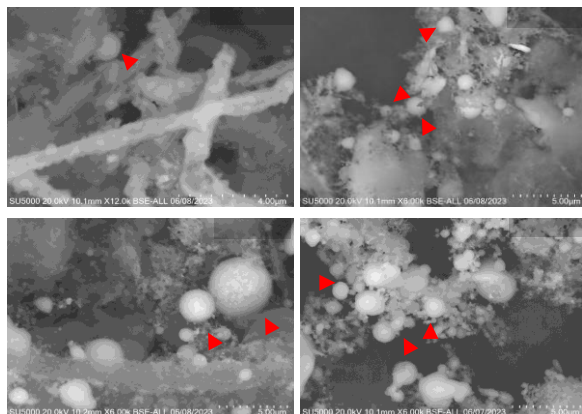
Box 1

Figure 1

SEM micrographs of the 4 samples

Source: Own elaboration

As can be seen in the 4 micrographs corresponding to different synthesis times, indicated in the upper right part, several nanostructures with deformity in their upper layer are observed, but in all of them nanospheres of different sizes appear.

It can be confirmed that the amount of these structures and their shapes vary with time. For example, in the micrograph taken at 2.5 minutes, more nanotubes or nanowires than nanospheres are observed, unlike the micrographs taken at 10 minutes, where more nanospheres are present and no other form of carbons can be seen.

Another important aspect to highlight is the size of these nanostructures. In the case of micrographs taken at 2.5 minutes, it is observed that the nanospheres have an average diameter of about 380 nanometers at 1.1 microns. In the micrographs taken at 5 minutes, the nanospheres have an average diameter of about 980 nanometers at 1.68 microns.

For micrographs taken at 7.5 minutes, nanospheres with diameters of 4.66 nanometers to 1.31 microns are observed, while, at 10 minutes, the sizes vary from about 679 nanometers to 1.86 microns.

We conclude that the nanostructures become larger at higher synthesis time exposure and that the nanospheres can be defined as multilayered nanobeads, since they present not very smooth surfaces and some few uniform ones (Karthik,2014), moreover, they exceed the corresponding size to classify them among fullerenes and/or quantum dots (Georgakilas,2015. Yang,2023).

This is because as the synthesis time and therefore the temperature increases, there is more time for the carbon atoms to reorganize and form a larger and perhaps ordered structure (Zhao ,2005). The ceramic crucible used still plays a significant role in reaching a higher temperature in a longer time. However, it is important to keep in mind that the relationship between the synthesis time and the size of the nanospheres is not always linear, so it is intended to optimize the synthesis technique.

X-ray diffractometer

To corroborate the type of morphology of the nanostructures, an X-ray diffractometer brand X'Pert pro PANalytical with CuKα radiation λ=0.1542 nm was used. The plane references obtained yielded C60 and C70 fullerene-type carbon nanostructures, as shown in figure (2).

The presence of planes corresponding to these two types of fullerenes may be to the similarity that exists with nanorod-like nanostructures, due to the interactions with the outer layers of these, which usually resemble individual fullerenes (Zeiger,2023).

We can observe that the planes obtained in the sample at 2.5 minutes, have lower peak intensities and increases as the exposure time increases until reaching 10 minutes, only in the case of graphite peak ($2\theta=26°$), the intensity decreases as the synthesis time increases, this variation in intensity directly influences the crystallinity, shape, size, and structural defects (Terohid ,2018). The obtained planes confirm the presence of spherical nanostructures, possibly of multilayered nanosheets type with impurities in their outer layer, previously seen in SEM micrographs.

Box 2
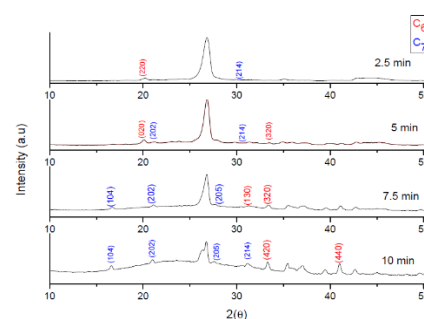
Figure 2

XDR of the 4 samples at different exposure times

Source: Own elaboration

Ordóñez-Casanova, Elsa Gabriela, Trejo-Mandujano, Héctor Alejandro, Saucedo-Acuña, Rosa Alicia and Villanueva-Montellano, Alfredo. [2024]. Morphological analysis and its effect on the optical properties of carbon nanospheres as a function of synthesis time. Journal of Systematic Innovation. 8[22]1-7: e1822107.
https://doi.org/10.35429/JSI.2024.8.22.1.7

UV-Vis Absorption spectroscopy

Optical properties were observed using a Stellar et spectrometer with a Newport integrated sphere to obtain UV-VIS Figure 3. The absorbance of carbon nanostructures can be present in several regions of the electromagnetic spectrum, but for our analysis we will focus only on the electronic transitions π→π* (200 - 400 nm) and n→π* (400 nm -750 nm) (Orlandi,2002).

The absorbance spectra of the 4 samples present the absorption behavior of very similar nanostructures to C60 and C70 (Duarte-Ruiz,2021) which are very similar to nanorod responses.

In the region of electronic transitions π→π corresponding to the ultraviolet-visible UV-Vis region, repetitive responses were observed in the 4 samples, considering the most notable peaks at: 223,270,340,392 nm, this indicates the presence of nanostructures of different sizes (Duarte-Ruiz,2021).

In the region of electronic transitions n→π* corresponding to the visible region, the most remarkable repetitive peaks would be: 433,453,516 and 530 nm, indicating larger nanostructures. According to the literature, the similarity of responses of nanostructures such as C60 has strong absorption bands in the ultraviolet region of the spectrum, typically around 200 to 350 nm and the C70 shows strong absorption bands in the UV region (Duarte-Ruiz,2021).

With this absorption behavior of the graph, we confirm the presence of spherical nanostructures of different sizes visualized in SEM micrographs, more like nano-onions.

Box 3
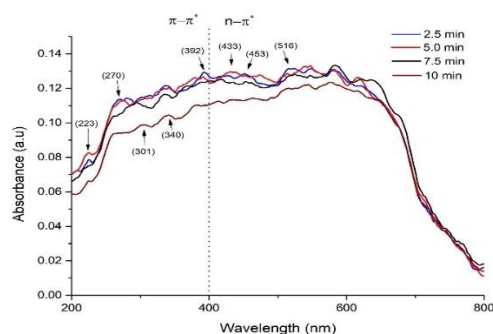
Figure 3

UV-vis absorption spectra of the four samples obtained
Source: Own elaboration

Optical band gap estimation

In Graph 4, the estimated behavior of the optical energy gap of the 4 samples obtained by the Tauc method from the analysis of the absorption data, Graph 3 is shown (Tauc,1968). It is widely recognized that this method assumes that the absorption coefficient is dependent on the photon energy (α) and can be expressed by the following equation [1]:

$$(\alpha - hv)^{\wedge}\left(1/\gamma\right) = B(hv - Eg) \qquad [1]$$

where h is Planck's constant, ν is the photon frequency, Eg is the band gap energy, and B is a constant (Tauc,1968).

Box 4
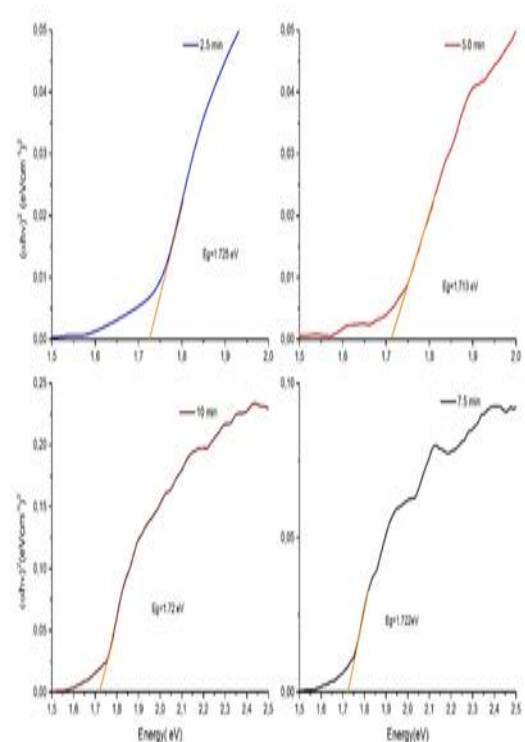
Figure 4

Optical band gap estimation of the four samples
Source: Own elaboration

It is observed in the graph that the band gaps vary very little, remaining on average at 1.70 ev. This value is consistent with the energy gaps of semiconductor powders, corresponding to unfunctionalized nanoparticles whose gap energy is around 1.6-1.7ev and corresponding to C60 and C70 carbon nanostructures (Rabenau, 1993).

Ordóñez-Casanova, Elsa Gabriela, Trejo-Mandujano, Héctor Alejandro, Saucedo-Acuña, Rosa Alicia and Villanueva-Montellano, Alfredo. [2024]. Morphological analysis and its effect on the optical properties of carbon nanospheres as a function of synthesis time. Journal of Systematic Innovation. 8[22]1-7: e1822107.
https://doi.org/10.35429/JSI.2024.8.22.1.7

With respect to the behavior of the curves, it is evident that at temperatures above 2.5 minutes, they show a distortion in the linearity of the graph considered as extended tail, which confirms the presence of structural defects and impurities (Makuła et al.,2018).

These defects usually appear in materials that have suffered damage or modifications in their upper layer which causes additional energy states to be introduced (Makuła et al.,2018), causing the spectrum Estimation of the Optical Band Gap of the Four Samples having a similarity with the so-called Urbach tails (Migliorini,2022).

Only in the case of the time at 2.5 minutes, the graph presents a linearity without distortion, if we observe the micrograph, it is possible that it is because of the presence of more carbon nanostructure shapes (tubes, threads, spheres, etc.) and as the synthesis time was shorter, perhaps they did not obtain very little structural damage.

Conclusions

In this work, we presented the morphological study and the behavior of the optical properties of carbon nanostructures of the nanoshells, obtained by a simple and economic method, with short synthesis time variations. It was observed that the carbon nanoparticles with longer synthesis time present more structural damage in their morphology, and their optical responses showed no significant variations across different synthesis times.

We believe this work is pertinent because the method is feasible and easily reproducible, which can be optimized to produce nanoparticles with fewer structural defects for specific applications.

Declarations

Conflict of interest

The authors declare no conflict of interest. They have no known competing financial interests or personal relationships that could have appeared to influence the work reported in this article.

Author contribution

Ordoñez-Casanova, Elsa G.: Contributed to the development of the project concept, research methodology, and experimental techniques, including the synthesis of carbon nanospheres.

Trejo-Mandujano, Héctor A: Contributed to the development of the project concept, research methodology, and experimental techniques, including morphological characterization using SEM and XRD.

Saucedo-Acuña, Rosa A: Contributed to the development of the optical analysis using UV-Vis spectroscopy and the Tauc method.

Villanueva Montellano, Alfredo: Contributed to manuscript writing, data interpretation, and the formulation of conclusions

Availability of data and materials

Data sets used or analyzed during the current study are available from the corresponding author upon reasonable request.

Funding

The research did not receive any funding.

Abbreviations

C60	Nanostructure composed of 60 carbon atoms
C70	Nanostructure composed of 70 carbon atoms
SEM	Scanning electron microscopy
XRD	X-ray diffraction

References

Antecedents

Ordoñez-Casanova, Elsa G., Manuel Román-Aguirre, Alfredo Aguilar-Elguezabal, and Francisco Espinosa-Magaña. (2013). Synthesis of Carbon Nanotubes of Few Walls Using Aliphatic Alcohols as a Carbon Source. *Materials,* 6,2534-2542.

Ordoñez Casanova, E. G., Trejo Mandujano, H. A., & Aguirre, M. R. (2019). Microscopy and spectroscopy characterization of carbon nanotubes grown at different temperatures using cyclohexanol as carbon source . *Journal of Spectroscopy*, *2019*(1), 6043523.

Adeola, A. O., Duarte, M. P., & Naccache, R. (2023). Microwave-assisted synthesis of carbon-based nanomaterials from biobased resources for water treatment applications: emerging trends and prospects *Frontiers in Carbon*, *2*, 1220021.

Pawelski, D., & Plonska-Brzezinska, M. E. (2023). Microwave-Assisted Synthesis as a Promising Tool for the Preparation of Materials Containing Defective Carbon Nanostructures: Implications on Properties and Applications *Materials*, *16*(19), 6549.

Zhou, J., Xu, W., You, Z., Wang, Z., Luo, Y., Gao, L., ... & Lan, L. (2016). A new type of power energy for accelerating chemical reactions: the nature of a microwave-driving force for accelerating chemical reactions. *Scientific reports*, *6*(1), 25149.

Masi, C. A., Schumacher, T. A., Hilman, J., Dulal, R., Rimal, G., Xu, B., ... & Chien, T. (2021). Converting raw coal powder into polycrystalline nano-graphite by metal-assisted microwave treatment . *Nano-Structures & Nano-Objects*, *25*, 100660.

De Medeiros, T. V., Manioudakis, J., Noun, F., Macairan, J. R., Victoria, F., & Naccache, R. (2019). Microwave-assisted synthesis of carbon dots and their applications. *Journal of Materials Chemistry C*, *7*(24), 7175-7195.

Basics

Siebert, J. P., Hamm, C. M., & Birkel, C. S. (2019). Microwave heating and spark plasma sintering as non-conventional synthesis methods to access thermoelectric and magnetic materials *Applied Physics Reviews*, *6*(4).

Kumar, A., Kuang, Y., Liang, Z., & Sun, X. (2020). Microwave chemistry, recent advancements, and eco-friendly microwave-assisted synthesis of nanoarchitectures and their applications: a review *Materials Today Nano*, *11*, 100076.

Dankovich, T. A. (2014). Microwave-assisted incorporation of silver nanoparticles in paper for point-of-use water purification *Environmental Science: Nano*, *1*(4), 367-378.

Ashok, C. H., Rajendar, V., Rao, K. G., Rao, K. V., & Chakra, C. S. (2014). Microwave-assisted method for zno nanoparticles synthesis using ionic liquids.

Zhu, L. J., Miao, H., Liu, K., Sun, Y. G., Qiu, M., & Zhu, X. C. (2012). Microwave and conventional hydrothermal synthesis of TiO2 nanoparticles and their photocatalytic activities *Advanced Materials Research*, *391*, 988-992.

Pati, S. S., Kalyani, S., Mahendran, V., & Philip, J. (2014). Microwave assisted synthesis of magnetite nanoparticles. *Journal of Nanoscience and Nanotechnology*, *14*(8), 5790-5797.

Borrell, A., Salvador, M. D., Peñaranda-Foix, F. L., & Cátala-Civera, J. M. (2013). Microwave sintering of zirconia materials: mechanical and microstructural properties. *International Journal of Applied Ceramic Technology*, *10*(2), 313-320.

Kuo, H. N., Chou, J. H., & Liu, T. K. (2016). Microstructure and mechanical properties of microwave sintered ZrO2 bioceramics with TiO2 addition *Applied bionics and biomechanics*, *2016*(1), 2458685.

Supports

Karthik, P. S., Himaja, A. L., & Singh, S. P. (2014). Carbon-allotropes: synthesis methods, applications and future perspectives *Carbon letters*, *15*(4), 219-237.

Georgakilas, V., Perman, J. A., Tucek, J., & Zboril, R. (2015). Broad family of carbon nanoallotropes: classification, chemistry, and applications of fullerenes, carbon dots, nanotubes, graphene, nanodiamonds, and combined superstructures. *Chemical reviews*, *115*(11), 4744-4822.

Yang, H. L., Bai, L. F., Geng, Z. R., Chen, H., Xu, L. T., Xie, Y. C., ... & Wang, X. M. (2023). Carbon quantum dots: Preparation, optical properties, and biomedical applications. *Materials Today Advances*, *18*, 100376.

Zhao, Z. G., Ci, L. J., Cheng, H. M., & Bai, J. B. (2005). The growth of multi-walled carbon nanotubes with different morphologies on carbon fibers. *Carbon*, *43*(3), 663-665.

Zeiger, M., Jäckel, N., Mochalin, V. N., & Presser, V. (2016). Carbon onions for electrochemical energy storage *Journal of Materials Chemistry A*, *4*(9), 3172-3196.

Terohid, S. A. A., Heidari, S., Jafari, A., & Asgary, S. (2018). Effect of growth time on structural, morphological and electrical properties of tungsten oxide nanowire *Applied Physics A*, *124*, 1-9.

Orlandi, G., & Negri, F. (2002). Electronic states and transitions in C 60 and C 70 fullerenes *Photochemical & Photobiological Sciences*, *1*(5), 289-308.

Duarte-Ruiz, A., Torres-Cortés, S. A., Meléndez, A., Velásquez, J. D., & Chaur, M. N. (202 Synthesis and characterization of C60 and C70 acetylace-tone monoadducts and study of their photochemical properties for potential application in solar cells *Revista Colombiana de Química*, *50*(1), 86-97.

Tauc, J. (1968). Optical properties and electronic structure of amorphous Ge and Si *Materials research bulletin*, *3*(1), 37-46.

Difference

Rabenau, T., Simon, A., Kremer, R. K., & Sohmen, E. (1993). The energy gaps of fullerene C60 and C70 determined from the temperature dependent microwave conductivity. *Zeitschrift für Physik B Condensed Matter*, *90*(1), 69-72.

Makuła, P., Pacia, M., & Macyk, W. (2018).

How to correctly determine the band gap energy of modified semiconductor photocatalysts based on UV–Vis spectra *The journal of physical chemistry letters*, *9*(23), 6814-6817.

Migliorini, F., Belmuso, S., Dondè, R., De Iuliis, S., & Altman, I. (2022). To optical properties of carbon nanoparticles: A need in comprehending Urbach energy. *Carbon Trends*, *8*, 100184.

Article

Innovative Ti/Fe/Eu-Carbon composite for Cephalexin adsorption

Compósito innovador de Ti/Fe/Eu-Carbón para la adsorción de cefalexina

Gómez-Vilchis, J.C.*[a], García-Rosales, G.*[b], Lóngoria-Gándara, L.C.[c] and Tenorio-Castilleros, D. [d]

[a] ROR Tecnológico Nacional de México – Instituto Tecnológico de Toluca• LKK-0328-2024 • 0000-0002-1023-9651 • 957883

[b] ROR Tecnológico Nacional de México – Instituto Tecnológico de Toluca • LKK-5096-6657 • 0000-0003-4438-6657 • 43369

[c] ROR International Atomic Energy Agency • 0000-0001-8524-9777

[d] ROR Instituto Nacional de Investigaciones Nucleares• 0000-0001-7742-2437 • 5288

CONAHCYT classification:

Area: Physics-Mathematics and Earth Sciences
Field: Physics
Discipline: Physics of the solid state
Subdiscipline: Composite materials

Abstract

The study focused on developing an innovative material for the adsorption of antibiotics in contaminated water. A biochar modified with titanium (Ti), iron (Fe), and europium (Eu) (Ti/Fe/Eu-Carbon) was synthesized to adsorb cephalexin (CEX) from aqueous solutions. The biochar was characterized using techniques such as SEM, EDS, and XPS, which confirmed the presence and energy states of Ti, Fe, and Eu. The material exhibited an impressive specific surface area of 232 $m^2 g^{-1}$ and a mesoporous structure. Adsorption experiments revealed that CEX adsorption occurs through both physisorption and chemisorption, achieving a maximum adsorption capacity of 600 $\mu g g^{-1}$, compared to 90 $\mu g g^{-1}$ for unmodified biochar. Optimal adsorption conditions were identified at pH 7 and a temperature of 20°C, as the process was found to be exothermic and spontaneous. Furthermore, the material demonstrated reusability for up to eight cycles.
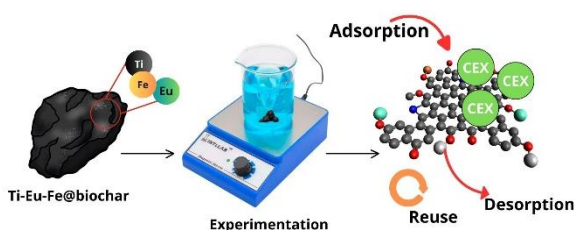
Adsorption, Composite, cephalexin.

Resumen

El estudio se centró en el desarrollo de un material innovador para la adsorción de antibióticos en aguas contaminadas. Se sintetizó un biocarbón modificado con titanio (Ti), hierro (Fe) y europio (Eu) (Ti/Fe/Eu-Carbón) para adsorber cefalexina (CEX) de soluciones acuosas. El biocarbón fue caracterizado mediante técnicas como SEM, EDS y XPS, las cuales confirmaron la presencia y los estados energéticos de Ti, Fe y Eu. El material mostró una notable área superficial específica de 232 $m^2 g^{-1}$ y una estructura mesoporosa. Los experimentos de adsorción revelaron que la adsorción de CEX ocurre a través de procesos de fisisorción y químisorción, alcanzando una capacidad máxima de adsorción de 600 $\mu g g^{-1}$, en comparación con los 90 $\mu g g^{-1}$ del biocarbón no modificado. Las condiciones óptimas de adsorción se identificaron a pH 7 y a una temperatura de 20°C, ya que el proceso resultó ser exotérmico y espontáneo. Además, el material demostró ser reutilizable hasta en ocho ciclos.

Adsorción, Compósito, Cefalexina

RENIECYT
Registro Nacional de Instituciones y Empresas Científicas y Tecnológicas
I702902 CONAHCYT

Article

Introduction

In recent years, the use of antibiotics has increased significantly, leading to their presence as pollutants in rivers (Su et al., 2023), groundwater, lakes, wastewater (Durán-Álvarez et al., 2023), and, in some cases, drinking water (Wang et al., 2023). Excessive use of antibiotics results in the emergence of resistant bacteria (Jampani et al., 2024), and these substances can also be persistent, bioaccumulative, and toxic in the environment (Li et al., 2023).

Despite their environmental impact, antibiotics are crucial for treating a wide range of infections caused by both Gram-negative and Gram-positive bacteria (Ali et al., 2023). Among the most used antibiotics is cephalexin, a β-lactam derivative (Gou et al., 2021) used to treat urinary tract infections, respiratory tract infections, and other common bacterial infections (Bailey et al., 1970).

Due to their presence in wastewater effluents, new methods are sought for their removal, including membrane bioreactors, phytoremediation, photodegradation, and adsorption, among others. However, adsorption has been extensively studied due to its ease of operation, low cost, and reusability.

Among, the most efficient adsorbent materials are composites, which are matrices loaded with particles that enhance their physical and chemical properties (Wang et al., 2022). This is due to significant increases in surface area, stability, resistance, and thermal conductivity. Chemically modified biocarbons are used as composites, particularly those loaded with metal oxides and salts.

For example, the presence of iron (Fe_2O_4) and titanium (TiO_2) oxides has been reported to facilitate the formation of oxygen-rich functional groups, leading to the creation of mesopores and an increased surface area (Liang et al., 2024; Nakarmi et al., 2022; Guo et al., 2022).

Lanthanide-based compounds have gained popularity in recent years due to their stability across various pH ranges and excellent chemical stability (Kajjumba et al., 2022).

The presence of metal and lanthanide oxides has shown favorable results, as demonstrated by Gong et al. (2024), because they enhance pollutant retention through functional groups on the surface, improving adsorption capacity.

Additionally, these compounds, when supported in small amounts on biocarbon, can achieve up to 98% efficiency due to the formation of active sites on the surface (Lan et al., 2022) which create new oxygen vacancies (Lin et al., 2018), particularly with europium due to its oxidation states (2^+ or 3^+).

Due to their physical and chemical properties, binary and ternary metal oxide systems attract significant attention as potential agents for removing emerging contaminants (Lǚ et al., 2013).

Consequently, metal and lanthanide oxide particles supported on biocarbon present a promising material for cephalexin removal due to their efficiency and low production cost.

In this study, a composite with Ti, Fe, Eu particles supported on biocarbon was synthesized for the removal of cephalexin in aqueous phase, evaluating the effects of various parameters such as time, initial concentration, pH, and temperature. Its ease of preparation, combined with its versatility, offers significant advantages for future use in treating antibiotic-contaminated waters.

Methodology

Materials

To prepare the composite, preconditioned avocado pits were used along with the following reagents: HNO_3 (J.T Baker®, 70%), NaOH (Fermont®), C_2H_6O (J.T Baker®, 99%), $Ti[OCH(CH_3)_2]_4$ (Sigma-Aldrich®, 97%), $Fe(NO_3)_3 \cdot 9H_2O$ (Sigma-Aldrich®, 98%), $Eu(NO_3)_3 \cdot 5H_2O$ (Sigma-Aldrich®) and a Cephalexin standard (1000 mg L^{-1}) (Sigma-Aldrich®), from which the solutions were prepared.

Preparation of Ti/Fe/Eu-Carbon composite

The avocado seeds were repeatedly washed with distilled water to remove impurities and then dried at room temperature for 72 h.

The dried seeds were ground and sieved to obtain a particle size of 0.83 mm. The powdered material was washed several times with hot water and then dried at 40°C for 24 h.

To prepare the composite, 10 mL of C_2H_6O was added to a reactor and stirred continuously at 30°C. Gradually, 350 µL of a $Ti[OCH(CH_3)_2]_4$ solution was added dropwise. The mixture was stirred for 15 min at 70°C, after which 10 mL each of $Fe(NO_3)_3 \cdot 9H_2O$ and $Eu(NO_3)_3 \cdot 5H_2O$ solutions (0.03 M) were added.

Finally, 3 grams of avocado seed powder were introduced into the reactor, which was then sealed and placed in a temperature-controlled shaking bath at 50°C for 12 h. After the reaction, the impregnated material was pyrolyzed at 650°C for 3 h. The resulting composite was named Ti/Eu/Fe-Carbon.

Morphological and Surface Characterization

To analyze the morphology of the material, a JEOL® JSM-5900 LV scanning electron microscope was used, equipped with an OXFORD® INCAx-Act 51-ADD0013 probe for elemental analysis. This analysis was conducted across five different areas.

The isoelectric point (IP) of the material was determined by placing 0.005, 0.05, 0.1, 0.15, 0.25, 0.35, 0.45, 0.55, and 1 g of the material into polypropylene tubes, each containing 10 mL of deionized water at 25°C. The tubes were stirred continuously for 24 h. The pH was then measured in each tube using a HANNA Instruments® potentiometer, and the data were plotted.

To determine the specific surface area, pore volume, and average pore size of the composite, a Belsorp Max III instrument was used in a nitrogen environment. The sample underwent a degassing pretreatment for 2 h at 200°C using a Belpre II instrument. The density of active sites was assessed following the methodology reported by Hayes et al., (1991).

Energy state analysis was performed using the Thermo Scientific K-Alpha X-Ray Photoelectron Spectrometer®, equipped with an Al (Kα) X-ray source. The instrument conducted 10 scans per sample in normal lens mode, with an aperture size of 400 µm and a step size energy of 0.030 eV.

Adsorption Experiments

To assess the adsorption capacity of CEX for the composite, kinetic and adsorption isotherm experiments were also conducted with carbon without Ti/Fe/Eu, to use it as a blank (BC) and evaluate its contribution to the process. A 500 µg L^{-1} solution of CEX was used, and the experiments were carried out using batch methodology, with CEX residues quantified using a Perkin Elmer® Lambda 35 UV-Vis spectrophotometer at λ = 250 nm.

The CEX adsorption kinetics were studied using polyethylene tubes with 1 mg of material each and 5 mL of a CEX solution at 200 µg L^{-1}. Experiments were conducted at different contact times: 5, 10, 30 min, 1, 2, 3, 6, 9, 12, 15, 18, and 24 h. The tubes were agitated in a temperature-controlled shaking bath at 20, 30, and 40 °C and pH=7. The data obtained were fitted to the Lagergren, Ho-Mackay, and Elovich mathematical models.

For the adsorption isotherms, the same conditions were used with different CEX concentrations (150, 160, 170, 180, 190, 200, 220, and 240 µg L^{-1}), with agitation for 24 h at 20, 30, and 40 °C and pH = 7. The data obtained were fitted to the Langmuir, Freundlich, and Temkin mathematical models.

The adsorption capacity q_e (µg g^{-1}) was calculated using Equation 1.

$$q_e = \frac{(C_0 - C_e)\, V}{M} \qquad [1]$$

Where C_0 (µg L^{-1}) (µg L^{-1}) is the initial concentration, and C_e is the equilibrium concentration; M (g) is the weight of the adsorbent material, and V (L) is the volume of the solution.

On the other hand, to evaluate the adsorption capacity of the materials as a function of pH, polypropylene tubes were used. Each tube contained 1 mg of material and 5 mL of the CEX solution. The initial pH was adjusted by adding small volumes of HNO_3 and/or NaOH (0.1 M).

The experiments were conducted across a pH range of 2 to 12 at 20, 30, and 40 °C, with continuous agitation for 24 h. Afterward, each tube was centrifuged at 2500 rpm for 3 min and the concentration was determined using UV-vis spectroscopy.

To determine reuse cycles, regeneration tests were conducted by subjecting the adsorbent material to a desorption process for 1 h in an acidic medium (pH=2) using 0.1 M HNO₃. Subsequently, 1 mg of each material was reintroduced into a contaminant solution at 20 °C and pH = 7, and this procedure was repeated until the minimum adsorption percentages were achieved.

Results

Characterization

The characterization of the composite, presented in Fig. 1a, shows a structure with semicircular cavities approximately 40 µm in diameter, whose rough walls may facilitate the diffusion of contaminants within the material. This type of structure is relevant for applications where accessibility and distribution of the contaminant within the material are crucial, as the cavities can serve as sites for accumulation and adsorption.

Within these cavities, as shown in Fig. 1b, there are small spherical particles with an average diameter of 1.8 ± 0.3 µm, forming clusters (Fig. 1c) with an elemental composition of C (77.82%), O (19.55%), Ti (0.89%), Fe (0.84%), and Eu (0.90%). These particles correspond to the titanium, iron, and europium oxides formed in the composite. The presence of these particles is consistent with findings reported by Fazal et al. (2020) and Viglašová et al. (2020), who observed similar morphologies in metal oxide compounds.

This validates that the synthesis method used produces a material with the expected morphology and functionality for adsorption applications. Fig. 1d shows the effect of the CEX adsorption process on the Ti/Eu/Fe-Carbon composite. While the general morphology remains similar, deformation in the cavities is observed, with tighter folds in the walls. This deformation may result from the adsorption process, which could induce structural changes in the material. However, the persistence of the spherical particles ((C (82.36%), O (16.38%), Ti (0.35%), Fe (0.48%), and Eu (0.43%)) indicates that, despite the morphological changes, the fundamental characteristics of the composite remain intact.

Regarding the elemental composition, the carbon (C) percentage increases from 77.82% to 82.36% after adsorption, while the percentages of oxygen (O), titanium (Ti), iron (Fe), and europium (Eu) decrease. The increase in carbon content may be attributed to the adsorption of CEX on the material's surface, which raises the proportion of carbon in the elemental analysis. The decrease in other elements may reflect the specific interaction between the material and the contaminant, altering the relative proportions of the detected elements. This is consistent with findings by Nawas et al. (2023), which suggest that interactions between the material and the contaminant can alter the observed elemental composition.

Box 1
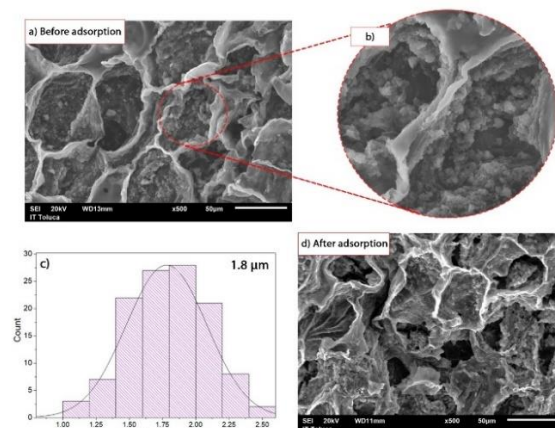
Figure 1

a) Micrograph of Ti/Eu/Fe-Carbon; b) Formation of spherical particles; c) Particle size distribution; d) Post-adsorption of CEX

The specific surface area of Ti/Eu/Fe-Carbon, which is 232 m²/g, exceeds that reported for other biochars modified with iron and lanthanide oxides, as noted in the studies by Fan et al. (2021) and Yaghini & Faghihian (2020). A similar value is reported by Wang et al. (2023).

This increase in surface area can be attributed to the presence of metal oxide particles in the material, which enhance the surface area due to increased dispersion and the formation of a more porous structure.

Ti/Eu/Fe-Carbon is classified as mesoporous, with a pore diameter of 2.69 nm. According to IUPAC definitions, mesoporous materials have pore sizes ranging from 2 to 50 nm (Mangeli et al., 2021). Additionally, the material has a pore volume of 0.1565 cm³ g⁻¹.

The presence of mesopores in the material is beneficial for adsorption, as it facilitates greater contact between the material's surface and contaminants, promoting better diffusion of these contaminants to the active surface.

The number of active sites, calculated from the specific surface area, is 20 sites nm^{-2}, indicating a high density of available sites for adsorption. This value is crucial for assessing the material's capacity to capture and retain contaminants.

The isoelectric point (IP) of Ti/Eu/Fe-Carbon was determined to be at a pH of 8. This pH is where the material's charges are in equilibrium, meaning the material has no net charge. An IP of 8 is consistent with values reported for some biochars (D'Cruz et al., 2020). Below this pH, the material's surface charge is positive due to an excess of [H$^+$] ions, while above this pH, the charge is negative due to an excess of [OH$^-$] ions.

These results are similar to those reported by Chen et al. (2023) in a ternary Fe-Ca-La compound and Cheng et al. (2023) in a Ca-Al-La compound.

These findings are promising for the adsorption of CEX, as the chemical speciation of CEX varies with pH, which can influence its adsorption capacity on the material (Watanabe et al., 2010). The well-defined IP and high specific surface area make Ti/Eu/Fe-Carbon an effective candidate for adsorption applications, as it can adapt to pH changes and provide high adsorption capacity due to its mesoporous structure and high density of active sites.

Adsorption experiments

In Fig. 2a, the comparison between Ti/Eu/Fe-Carbon and white Carbon (BC) shows a significant increase in adsorption capacity, rising from 90 to 560 µg L^{-1}. This substantial improvement suggests that the addition of Ti/Eu/Fe greatly enhances the adsorption efficiency of BC. This positive effect can be attributed to the presence of metal oxides, which appear to enhance the material's adsorptive properties. Fig. 2b presents the kinetic data for CEX adsorption onto the materials.

The maximum adsorption capacity is achieved at 560 µg L^{-1} at 20 °C. Adsorption efficiency is high from the first minutes of contact but decreases over time until equilibrium is reached in 1 h. This behavior is due to the progressive reduction in active sites (H$^+$, OH$^-$) on the materials and the decreasing concentration of CEX in the solution.

The decrease in the adsorption rate over time indicates that the active sites become saturated with CEX molecules, leading to an equilibrium state (Mishra et al., 2023). This behavior is comparable to that observed in the adsorption of pharmaceuticals such as venlafaxine, trazodone, and fluoxetine using eucalyptus-derived biochar (Puga et al., 2022).

The high initial adsorption rate is consistent with findings by Lu & Zhao (2024), who reported similar results using biochar derived from fish scales and pine needles for ciprofloxacin adsorption.

It is also observed that the adsorption capacity decreases with increasing temperature, suggesting that the adsorption process is exothermic. This phenomenon may be explained by the ability of CEX molecules to gain sufficient thermal energy to overcome the activation barrier and bind more effectively to the biochar surface, enhancing the adsorbent-adsorbate interaction (Azeez et al., 2024). Additionally, when CEX penetrates the internal pores of the biochars, these pores may become blocked, reducing the number of CEX molecules that can access the material.

To determine the influence of the initial concentration of CEX on the adsorption process and to identify the optimal time for maximizing the amount of adsorbed contaminant, adsorption isotherms are used. These isotherms allow for the evaluation of the adsorbents' capacity and performance by fitting experimental values to established mathematical models and comparing these models. Fig. 2c shows the behavior of CEX adsorption isotherms on the biochars, with adsorption capacities ranging from 600, 540, to 475 µg g^{-1}.

The decrease in adsorption capacity with increasing temperature may be attributed to CEX molecules having sufficient thermal energy to overcome the activation barrier and bind more effectively to the biochar surface, favoring the adsorbent-adsorbate interaction.

Gómez-Vilchis, J.C., García-Rosales, G., Lóngoria-Gándara, L.C. and Tenorio-Castilleros, D. [2024]. Innovative Ti/Fe/Eu-Carbon composite for Cephalexin adsorption. Journal of Systematic Innovation. 8[22]1-16: e2822116.
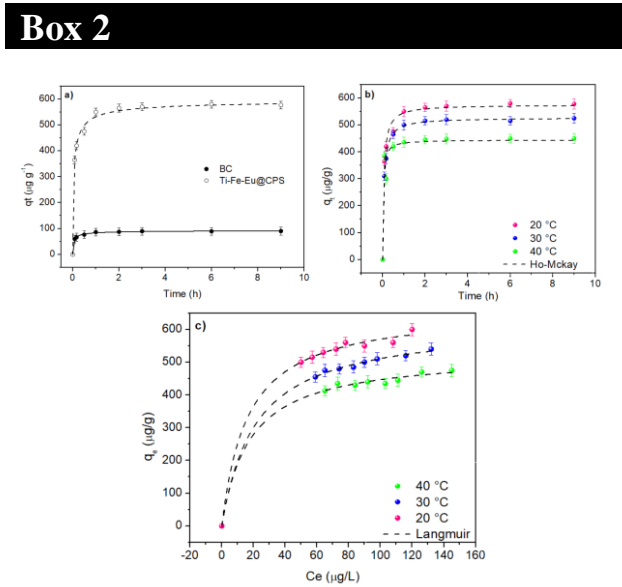https://doi.org/10.35429/JSI.2024.8.22.1.16

Box 2

Figure 2

a) Comparison of BC vs. Ti/Eu/Fe-Carbon b) kinetics and a) adsorption isotherms of CEX on Ti/Eu/Fe-Carbon at 20, 30 and 40 °C.

The kinetic adsorption data for CEX (Table 1) were fitted to various kinetic adsorption models (Lagergren, Ho-Mackay, and Elovich), with the best fit obtained using the Ho-Mackay model (Eq. 2), showing a correlation coefficient of 0.99-0.98 Ti/Eu/Fe-Carbon.

This suggests that in the CEX adsorption process, the reaction rate depends on the amount of solute adsorbed onto the adsorbent surface and the amount adsorbed at equilibrium (Ho et al., 1999).

This implies that the adsorption process is chemical in nature. These findings are consistent with the results reported by Wernke et al. (2020), who investigated CEX adsorption using graphene oxide, and Naghipour et al. (2019), who used a biocarbon derived from banana wood.

$$q_t = \frac{K_2 q_e^2 t}{1 + K_2 q_e t} \qquad [2]$$

Where q_e (mg g^{-1}), represents the adsorption capacity at equilibrium, and q_t (mg g^{-1}) represents the amount of solute adsorbed at time t (Oyekanmi et al., 2024).

Box 3

Table 1

Fitting of mathematical models for the adsorption kinetics of CEX on Ti/Eu/Fe-Carbon

T (°C)		20	30	40
Pseudo first order	$K_L (min^{-1})$	1597.1	1453.2	267.6
	q_e $(\mu g\ g^{-1})$	512.8	465.6	416.7
	R^2	0.8	0.7	0.8
Pseudo second order	K $(g\ \mu g^{-1}\ min^{-1})$	0.03	0.05	0.08
	q_e $(\mu g\ g^{-1})$	575	527	444.4
	R^2	**0.98**	**0.99**	**0.98**
Elovich	$A\ (\mu g\ g^{-1} min^{-1})$	5.90E+04	4.14E+04	3.98E+04
	$B\ (g\ \mu g^{-1})$	0.09	0.08	0.06
	R^2	0.98	0.98	0.97

The results of fitting the adsorption isotherms to the Langmuir, Freundlich, and Temkin mathematical models, presented in Table 2, indicate that the Langmuir model (Eq. 3) provides the best fit for the experimental data. Based on these findings and the XPS analysis, the proposed adsorption mechanism suggests that the adsorption of CEX onto Ti/Eu/Fe-Carbon involves both chemisorption and physisorption processes. In this mechanism, CEX molecules form chemical bonds with the adsorbent surface while also interacting through electrostatic forces (Moreroa-Monyelo et al., 2022).

The Langmuir model assumes that adsorption occurs at specific and homogeneous sites on the adsorbent surface, with each site accommodating only one molecule of adsorbate. The dimensionless parameter R_L, calculated as $R_L = 1/(1 + K_L Co)$, is used to interpret the nature of the adsorption process: $R_L > 1$ indicates unfavorable adsorption: $R_L = 1$ adsorption is linear; $R_L < 1$ the adsorption is favorable and R = 0 the adsorption is irreversible.

In this study, the R_L values are less than 1, demonstrating that the adsorption of CEX on Ti/Eu/Fe-Carbon is favorable. This indicates a strong affinity of the CEX molecule for the material's surface, facilitating its adsorption.

This finding supports the notion that chemisorption is the predominant mechanism in the interaction between CEX and the adsorbent.

Journal of Systematic Innovation

Article

$$q = \frac{q_0 y}{K_d + y} \qquad [3]$$

Where: q_0 is the maximum adsorption capacity of the adsorbent, K_d is the equilibrium constant, y is the concentration of solute in the solution, and q is the amount of solute adsorbed per unit of adsorbent (Fan et al., 2021).

Box 4

Table 2

Fitting of kinetic adsorption models for CEX on Ti/Eu/Fe-Carbon

T (°C)		20	30	40
Langmuir	q_m ($\mu g\ g^{-1}$)	892.7	883.4	878.8
	K_L ($L\ \mu^{-1}$)	-1.82 E+45	-4.56 E+44	-1.72 E+44
	R_L	-2.5E-48	-9.9E-48	-2.6E-47
	R^2	**0.99**	**0.99**	**0.98**
Freundlich	K_F ($\mu g\ g^{-1}$) ($L\ \mu g^{-1}$)$^{1/n}$	447.3	385.1	265.3
	n	0.37	0.39	0.53
	R^2	0.95	0.97	0.97
Temkin	q_m ($\mu g\ g^{-1}$)	7.17	6.24	5.41
	K_T ($\mu g\ L^{-1}$)	2.25	1.7	0.77
	R^2	0.93	0.92	0.95

In Table 3, the maximum sorption capacities (q_m) of CEX at different temperatures are compared with those reported in other studies. It is important to note that while the experimental conditions used vary, comparing q_m values remains valid as it provides insight into the performance of Ti/Eu/Fe-Carbon relative to other materials.

Some studies report higher adsorption capacities than those observed in this research. However, it is crucial to consider that many of these studies use larger amounts of adsorbent material for their adsorption experiments. In contrast, the advantage of the Ti/Eu/Fe-Carbon material lies in the fact that only 1 mg of adsorbent is used.

This suggests that despite the smaller amount of material, Ti/Eu/Fe-Carbon demonstrates a competitive or superior performance in adsorption capacity compared to other materials that require more adsorbent.

Box 5

Table 3

Comparison of CEX adsorption capacity in Ti/Eu/Fe-Carbon with literature values

Adsorbents	Adsorption capacity (q_m)	Co	Mass (mg)	Reference
Graphene oxide	164 mg g^{-1}	100	10	Wernke et al., 2020
Actived carbón	48 mg g^{-1}	50	-	Rashtbari et al., 2018
Bauxita	112 mg g^{-1}	300	10	Giannoulia et al., 2024
Biochar	57 mg g^{-1}	20	30	Acelas et al., 2021
Graphene	650 mg g^{-1}	700	-	Ali et al., 2023
Ti/Eu/Fe-Carbon	600 µg g^{-1}	0.2	1	This work

Impact of temperature on CEX adsorption onto Ti/Eu/Fe-Carbon

The study involved testing at different temperatures (20, 30, and 40 °C) to assess how temperature affects the adsorption process of CEX on Ti/Eu/Fe-Carbon. Temperature is a crucial factor in adsorption processes, as it can influence various properties of both the adsorbent and the adsorbate.

Firstly, temperature can impact the deprotonation of functional groups on the adsorbent's surface. This can lead to an increase in the concentration of hydroxyl groups (OH$^-$) on the surface, potentially altering the material's adsorption capacity. An increase in OH$^-$ groups might enhance the interaction between the adsorbent and the adsorbate, depending on the nature of the chemical interactions involved (Masulli et al., 2022).

Additionally, temperature affects the kinetic energy of the adsorbate molecules and their solubility in the solution. Higher temperatures increase the mobility of the molecules, facilitating their diffusion to the adsorbent's surface. This effect can improve the adsorption process's efficiency by allowing greater mass transfer (Wong et al., 2008).

An increase in temperature can also influence the reaction rate of the adsorption process. Chemical reactions typically accelerate with rising temperature due to increased kinetic energy, which can impact the reaction rate constant.

In aqueous solutions, temperature can affect the amount of dissolved molecular oxygen, which in turn can impact reactions involving oxygen (Karlsson et al., 2017; Groeneveld et al., 2023).

To quantify the effect of temperature on the adsorption rate, kinetic data were collected at the three mentioned temperatures and an Arrhenius plot was constructed. The plot was developed by plotting the natural logarithm of the rate constant (Ln k) against 1/T (K). The linearized form of the Arrhenius equation, shown in equation 5, allows for the calculation of activation energy and evaluation of how temperature affects the adsorption reaction rate (Eq. 5).

$$Lnk = \frac{Ea}{R}\left(\frac{1}{T}\right) + LnA \qquad [4]$$

Where k is the rate constant for the reaction at a given temperature, Ea is the activation energy for the process, R is the gas constant (8.314 kJ (mol·K)$^{-1}$), T is the temperature in Kelvin, and AAA is the frequency factor for the reaction.

As shown in Table 4, the thermodynamic parameters indicate that an increase in temperature reduces the interaction between the materials and the CEX molecule. The values for ΔH°, ΔS°, and ΔG° were determined using the equations provided (Eq. 5 and 6).

$$\Delta G° = \Delta H° - T\Delta S° \qquad [5]$$

$$Ln\ k = -\frac{\Delta°H}{R} * \frac{1}{T°} + \frac{\Delta S°}{R} \qquad [6]$$

Box 6

Table 4

Thermodynamic parameters obtained

T	Thermodynamic parameters			
(°C)	Ea (kJ mol^{-1})	ΔG° (kJ mol^{-1})	ΔH° (kJ mol^{-1})	ΔS° (J mol K^{-1})
20		-46.30	-19.75	-0.09
30	8.75E^{-05}	-47.20		
40		-48.11		

The activation energy (Ea) for CEX adsorption being greater than 40 kJ mol^{-1} suggests that the process involves chemisorption (Acelas et al., 2021).

This indicates that the adsorption is driven by strong chemical interactions between the adsorbate and the adsorbent. The negative values for ΔH° and ΔS° point to an increase in disorder at the liquid-solid interface and confirm that the adsorption process is exothermic.

This implies that the adsorption process releases heat and is accompanied by a decrease in the system's entropy (Imanipoor et al., 2020). As temperature increases, the binding potential at equilibrium decreases, leading to a reduction in sorption capacity (Gao et al., 2020). This trend aligns with the exothermic nature of the adsorption process, where higher temperatures can diminish the adsorbent's ability to bind the adsorbate effectively. Conversely, the negative values of ΔG° indicate a decrease in Gibbs free energy, demonstrating that the adsorption process is thermodynamically favorable and feasible through chemical interactions between the adsorbate and adsorbent (Kaya et al., 2024).

However, Fakhri et al. (2014) observed that an increase in temperature reduces CEX adsorption on carbonaceous materials, attributing this decrease to the exothermic nature of the process. This reduction can be explained by the weakening of Van der Waals forces between CEX molecules and the adsorbent material at higher temperatures (Wernke et al., 2020).

Effect of pH and adsorption mechanism of CEX on Ti/Eu/Fe-Carbon

In Fig. 3a, the data reveal that as pH increases, the percentage of CEX adsorbed rises up to pH 7, after which it starts to decline. This trend highlights the significant impact of pH on CEX adsorption efficiency. CEX exists in different ionic forms depending on the pH: cationic below pH 3, zwitterionic between pH 3 and 7, and anionic above pH 7 (Watanabe et al., 2010).

The increased adsorption observed between pH 5 and 7 aligns with the zwitterionic form of CEX, which has both positive and negative charges that interact favorably with the adsorbent surface.

The isoelectric point (IP) of the adsorbent material is 8. At pH levels below this IP, the adsorbent surface is positively charged, attracting the anionic forms of CEX.

Article

However, at pH levels lower than 3, the cationic form of CEX and the positively charged adsorbent create electrostatic repulsion, which reduces adsorption efficiency.

The significant adsorption at pH 5, consistent with findings from Rashtbari et al. (2020), supports the notion that the zwitterionic form of CEX shows a higher affinity for the adsorbent. This optimal pH range enhances the interaction between zwitterionic CEX and the adsorbent material. Between pH 4 and 6, increased adsorption is likely due to chemisorption, as indicated by previous kinetic studies.

At these pH levels, the zwitterionic CEX facilitates stronger chemical interactions with the adsorbent, leading to enhanced adsorption.

Beyond pH 7, where CEX becomes anionic, reduced adsorption is attributed to repulsion between the negatively charged CEX and the similarly charged or neutral adsorbent surface, leading to decreased interaction and adsorption efficiency. In summary, the adsorption of CEX is primarily influenced by its ionic form and the surface charge of the adsorbent material.

The data suggest that zwitterionic CEX, prevalent between pH 5 and 7, interacts most effectively with the adsorbent, thereby enhancing chemisorption and overall adsorption efficiency (Fig. 3b).

Box 7

a)
b)

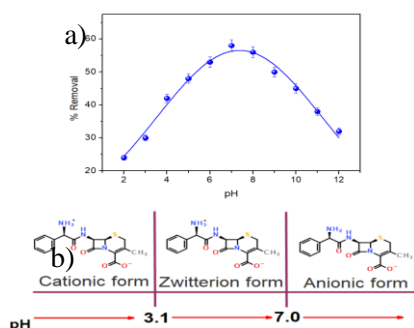Cationic form | Zwitterion form | Anionic form

pH   3.1   7.0

Figure 3

Effect of pH on the adsorption of CEX onto Ti/Eu/Fe-Carbon; b) Ionic species of CEX

In the context of cefalexin adsorption, X-ray photoelectron spectroscopy (XPS) has proven to be an essential tool for elucidating the energetic states on the surface of the Ti/Eu/Fe-Carbon material.

The XPS analysis identified various energetic states within the material's components, including C1s, O1s, N1s, Ti2p, Fe2p, and Eu3d, offering a detailed view of the chemical interactions relevant to cefalexin adsorption. In the C1s spectrum, with a full width at half maximum (FWHM) of 1.1 ± 0.1, several bands were observed, corresponding to different energetic states including C=C (aromatic), C-N, C-O, and C=O (carboxyl groups) (Fig. 4a) (Choi et al., 2019; Peng et al., 2017). These functional groups are crucial for interacting with cefalexin, as they can form specific bonds with the antibiotic, thereby enhancing its adsorption on the material's surface.

The O1s spectrum, with an FWHM of 1.4 ± 0.1, revealed energetic states associated with O-Metal, O=C, O-C, and O-C=O (Suo et al., 2021; Dodevski et al., 2017) (Fig. 4b). These oxygen states may play a key role in forming electrostatic interactions and hydrogen bonds with cefalexin, which could significantly influence its adsorption capacity. In the N1s spectrum, with an FWHM of 1.4 ± 0.1 (Fig. 4c), specific energetic states such as N-C and N=C were detected, related to pyridinic and pyrrolic nitrogen forms (Lawrie et al., 2007; Chen et al., 2014).

The presence of nitrogen could affect cefalexin adsorption through coordination bonds or acid-base interactions. The Ti2p analysis identified peaks corresponding to Ti^{4+} and Ti^{3+} at 464, 460, and 458 eV, respectively, indicating the presence of TiO_2 in the material (Kramar et al., 2024). The formation of TiO_2 could impact the material's adsorption capacity by modifying the surface and its reactivity (Fig. 4d).

In the Fe2p spectrum, peaks corresponding to Fe^{2+} at 709 eV and Fe^{3+} at 710.3 eV were detected (Rivera et al., 2020) (Fig. 4e). The oxidation states of iron may influence cefalexin interactions, potentially through ionic or redox mechanisms. Finally, the Eu3d spectrum showed two primary peaks at 1134.8 eV (Eu^{3+} 3d5/2) and 1126.2 eV (Eu^{2+} 3d5/2), along with two smaller satellite peaks at 1164.1 eV (Eu^{3+} 3d5/2) and 1155.5 eV (Eu^{2+} 3d3/2) (Brunckova et al., 2021) (Fig. 4f)

The presence of europium may impact the material's stability and its ability to adsorb cefalexin.

Gómez-Vilchis, J.C., García-Rosales, G., Lóngoria-Gándara, L.C. and Tenorio-Castilleros, D. [2024]. Innovative Ti/Fe/Eu-Carbon composite for Cephalexin adsorption. Journal of Systematic Innovation. 8[22]1-16: e2822116.
https://doi.org/10.35429/JSI.2024.8.22.1.16

In summary, XPS analysis provides a comprehensive understanding of the oxidation states and chemical interactions on the surface of the Ti/Eu/Fe-Carbon material. This detailed insight is crucial for optimizing the material's performance in cefalexin adsorption and other related processes.

Box 8
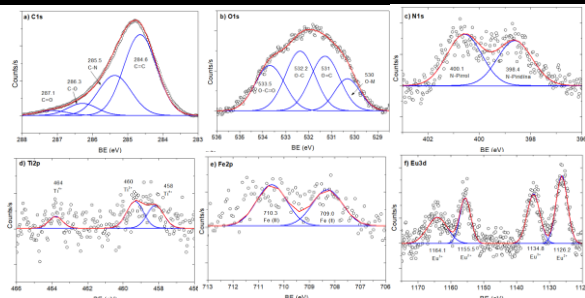
Figure 4

Deconvolution of a) C1s, b) O1s, c) N1s, d) Ti2p, e) Fe2p, and f) Eu3d

The proposed interaction mechanism between cefalexin (CEX) and the Ti/Eu/Fe-Carbon composite, illustrated in Figure 5 and supported by characterization results, adsorption isotherms, kinetic studies, and XPS data, offers a detailed understanding of the adsorption process.

The Ti/Eu/Fe-Carbon composite contains Ti, Fe, and Eu ions, which significantly contribute to CEX adsorption through electrostatic attractions. At pH 7, CEX exists in its dipolar form, possessing both positive and negative charges. The predominant oxidation states of titanium (Ti^{4+}, Ti^{3+}), iron (Fe^{2+}, Fe^{3+}), and europium (Eu^{3+}, Eu^{2+}) interact with water to form active sites such as OH^- and H^+. These sites exhibit a high affinity for the charges on the CEX molecule, promoting adsorption. For example, OH^- groups on the material can interact with the amino groups (NH_3^+) in CEX, facilitating the adsorption process (Cao et al., 2021).

Active H^+ sites on the material's surface can form hydrogen bonds with the oxygen atoms in the CEX molecule. Conversely, the amine groups in CEX can donate H^+ and form hydrogen bonds with the OH^- groups on the material's surface, a process known as hydrogen bonding (Ndoun et al., 2021). This interaction stabilizes CEX on the material's surface, enhancing adsorption.

The presence of aromatic rings in CEX is also crucial for adsorption capacity. The hexagonal structure of these rings facilitates adsorption onto carbon-based materials, with antibiotics having more aromatic rings adsorbing more rapidly due to π-π interactions (Acelas et al., 2021).

Additionally, hydrophobic C-C interactions are observed, where the methyl group in CEX interacts with methyl groups in Ti/Eu/Fe-Carbon. These interactions are driven by the hydrophobic nature of the involved groups (Krasucka et al., 2021). Furthermore, covalent C-O bonds are formed between the methyl group of CEX and the active OH^- sites on the material, further stabilizing and enhancing the adsorption process.

Based on our observations, the interaction mechanisms between CEX and the Ti/Eu/Fe-Carbon composite involve a combination of electrostatic attractions, hydrogen bonding, π-π interactions, hydrophobic interactions, and covalent bonding. Each of these mechanisms plays a crucial role in optimizing the adsorption of CEX onto the composite material, underscoring the importance of understanding and leveraging these interactions for effective adsorption.

Box 9
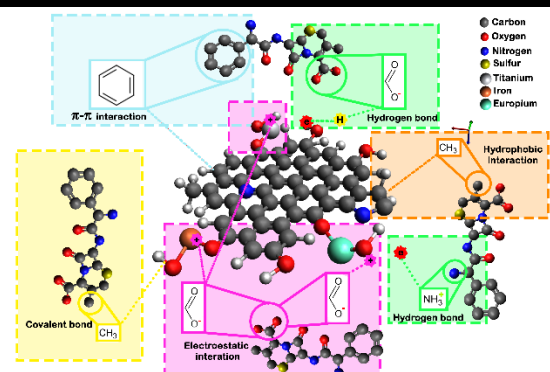
Figure 5

Mechanism of adsorption of CEX on Ti/Eu/Fe-Carbon

Reusability

Figure 6 depicts the percentage removal of cefalexin (CEX) by Ti/Eu/Fe-Carbon, which is used to assess the material's reuse and stability, crucial for evaluating its cost-effectiveness. For CEX desorption, an acidic solution with pH = 2 was employed since, at this pH, CEX is in its cationic form, which reduces its adsorption capacity.

Journal of Systematic Innovation

Article

The results reveal a decline in removal efficiency with each cycle of adsorption-desorption. Specifically, after 8 cycles, the removal efficiency decreased from 77% to 17% at 20°C, from 74% to 13% at 30°C, and from 70% to 12% at 40°C.

This performance drop indicates that the Ti/Eu/Fe-Carbon composite loses effectiveness over multiple cycles. Several factors might contribute to this decrease.

Repeated usage may deplete the active sites on the material, diminishing its adsorption capacity. Additionally, the acidic desorption environment and varying temperatures could affect the composite's structural integrity, further compromising its performance.

The substantial reduction in removal efficiency suggests that while Ti/Eu/Fe-Carbon may initially perform well, its long-term usability could be limited.

For practical applications, it is essential to address these issues and consider methods for regenerating or improving the material's stability to enhance its economic viability.
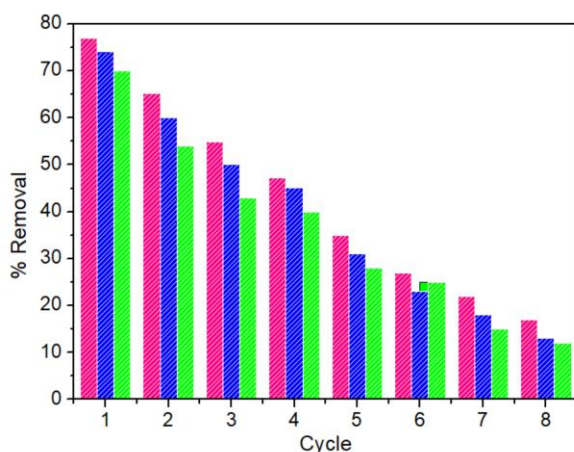
Box 10

Figure 6

Reusability cycles at 20, 30 and 40 °C of Ti/Eu/Fe-Carbon

Conclusions

The Ti/Eu/Fe-Carbon composite synthesized from avocado seeds presents a promising solution for addressing antibiotic contamination in water, specifically targeting cefalexin (CEX). This study highlights its effectiveness in removing CEX, achieving a notable removal efficiency of 80% ($160 \, \mu g \, L^{-1}$).

The composite's performance is optimized under specific conditions at 20°C, a pH of 7, and a contact time of 1 h demonstrating its efficiency and stability. The material's ability to be reused up to 8 times underscores its practical applicability and economic viability in water treatment processes.

The fitting of adsorption isotherms to the Langmuir, Freundlich, and Temkin mathematical models, as shown in Table 2, indicates that the Langmuir model (Eq. 3) provides the best fit for the experimental data. Based on these results and XPS analysis, the proposed interaction mechanism suggests that the adsorption of CEX onto Ti/Eu/Fe-Carbon involves both chemisorption and physisorption processes. In this mechanism, CEX molecules form chemical bonds with the adsorbent surface while also interacting through electrostatic forces (Moreroa-Monyelo et al., 2022).

Thermodynamic analysis reveals that the process is exothermic, with decreasing efficiency at higher temperatures, suggesting that the composite performs better in cooler conditions. This characteristic can be advantageous in specific environmental contexts or treatment scenarios.

Overall, this study underscores the potential of Ti/Eu/Fe-Carbon derived from avocado seeds as an innovative and effective material for mitigating antibiotic pollution. Its combination of high removal efficiency, reusability, and favorable adsorption properties makes it a valuable addition to the field of water treatment, offering a sustainable approach to combatting emerging environmental contaminants.

Declarations

Conflict of interest

The authors declare no conflicts of interest. They have no known financial or personal relationships that could have influenced the content of this article.

Author contribution

Gómez-Vilchis, J. C.: Conducted the experiments, analyzed and interpreted the data, and wrote the paper.

García-Rosales, G.: Designed and conceptualized the experiments, analyzed and interpreted the data, provided reagents, materials, analysis tools, or data, and contributed to writing and editing the article.

Longoria-Gándara, L. C.: Analyzed and interpreted the data and wrote the paper.

Tenorio-Castilleros, D.: Assisted with the analysis of several samples.

Availability of data and materials

The data are available and can be requested from the corresponding author.

Abbreviations

BC	Blank biochar
C	Carbon
CEX	Cephalexin
Ea	Activation energy
EDS	Energy Dispersive Spectroscopy
Eu	Europium
Fe	Iron
FWHM	The Full Width Half Maximum
G°	Gibbs free energy
H°	Enthalpy
IP	Isoelectric Point
N	Nitrogen
O	Oxygen
S°	Entropy
SEM	Scanning Electron Microscopy
Ti	Titanium
UV-Vis	UV-Visible Spectrophotometry
XPS	X-Ray Photoelectron Spectroscopy

References

Antecedents

Gong, W., Qi, C., Huang, L., Tian, Z., Huang, Z., Tao, C., Lin, H., Guo, L., & Yu, Z. (2024). Adsorption of phosphorus in wastewater by lanthanum-modified magnetic sewage sludge biochar. *Desalination and Water Treatment*, *320*, 100603.

Guo, D., Feng, D., Zhang, Y., Zhang, Z., Wu, J., Zhao, Y., & Sun, S. (2022). Synergistic mechanism of biochar-nano TiO_2 adsorption-photocatalytic oxidation of toluene. *Fuel Processing Technology*, *229*, 107200.

Liang, H., Zhu, C., Wang, A., & Chen, F. (2024). Facile preparation of $NiFe_2O_4$/biochar composite adsorbent for efficient adsorption removal of antibiotics in water. *Carbon Research*, *3*(1), 2.

Nakarmi, K. J., Daneshvar, E., Eshaq, G., Puro, L., Maiti, A., Nidheesh, P. V., Wang, H., & Bhatnagar, A. (2022). Synthesis of biochar from iron-free and iron-containing microalgal biomass for the removal of pharmaceuticals from water. *Environmental Research*, *214*, 114041.

Wang, G., Li, Y., Dai, J., & Deng, N. (2022). Highly efficient photocatalytic oxidation of antibiotic ciprofloxacin using TiO_2@g-C_3N_4@biochar composite. *Environmental Science and Pollution Research*, *29*(32), 48522-48538.

Basics

Azeez, L., Adefunke, O., Oyedeji, A. O., Agbaogun, B. K., Busari, H. K., Adejumo, A. L., Agbaje, W. B., Adeleke, A. E., & Samuel, A. O. (2024). Facile removal of rhodamine B and metronidazole with mesoporous biochar prepared from palm tree biomass: adsorption studies, reusability, and mechanisms. *Water Practice & Technology*, *19*(3), 730-744.

Bailey, A., Hadley, A., Walker, A., & James, D. G. (1970). Cephalexin a new oral antibiotic. *Postgraduate Medical Journal*, *46*(533), 157-158.

Brunckova, H., Mudra, E., Rocha, L., Nassar, E., Nascimento, W., Kolev, H., Kovalcikova, A., Molcanova, Z., Podobova, M., & Medvecky, L. (2021). Preparation and characterization of isostructural lanthanide Eu/Gd/Tb metal-organic framework thin films for luminescent applications. *Applied Surface Science*, *542*, 148731.

Cao, Y., Xie, X., Tong, X., Feng, D., Lv, J., Chen, Y., & Song, Q. (2021). The activation mechanism of Fe(II) ion-modified cassiterite surface to promote salicylhydroxamic acid adsorption. *Minerals Engineering*, *160*, 106707.

Chen, S., Cao, Y., & Feng, J. (2014). Polydopamine As an Efficient and Robust Platform to Functionalize Carbon Fiber for High-Performance Polymer Composites. *ACS Applied Materials & Interfaces*, *6*(1), 349–356.

Choi, S. W., Tang, J., Pol, V. G., & Lee, K. B. (2019). Pollen-derived porous carbon by KOH activation: Effect of physicochemical structure on CO_2 adsorption. *Journal of CO_2 Utilization*, *29*, 146–155.

Dodevski, V., Janković, B., Stojmenović, M., Krstić, S., Popović, J., Pagnacco, M. C., Popović, M., & Pašalić, S. (2017). Plane tree seed biomass used for preparation of activated carbons (AC) derived from pyrolysis. Modeling the activation process. *Colloids and Surfaces A: Physicochemical and Engineering Aspects*, *522*, 83–96.

Durán-Álvarez, J. C., Prado, B., Zanella, R., Rodríguez, M., & Díaz, S. (2023). Wastewater surveillance of pharmaceuticals during the COVID-19 pandemic in Mexico City and the Mezquital Valley: A comprehensive environmental risk assessment. *Science of The Total Environment*, *900*, 165886.

Gou, Y., Peng, L., Xu, H., Li, S., Liu, C., Wu, X., Song, S., Yang, C., Song, K., & Xu, Y. (2021). Insights into the degradation mechanisms and pathways of cephalexin during homogeneous and heterogeneous photo-Fenton processes. *Chemosphere*, *285*, 131417.

Hayes, K. F., Redden, G., Ela, W., & Leckie, J. O. (1991). Surface complexation models: An evaluation of model parameter estimation using FITEQL and oxide mineral titration data. *Journal of Colloid and Interface Science*, *142*(2), 448-469.

Ho, Y. S., & McKay, G. (1999). Pseudo-second order model for sorption processes. *Process Biochemistry*, *34*(5), 451-465.

Jampani, M., Mateo-Sagasta, J., Chandrasekar, A., Fatta-Kassinos, D., Graham, D. W., Gothwal, R., Moodley, A., Chadag, V. M., Wiberg, D., & Langan, S. (2024). Fate and transport modelling for evaluating antibiotic resistance in aquatic environments: Current knowledge and research priorities. *Journal of Hazardous Materials*, *461*, 132527.

Kajjumba, G. W., & Marti, E. J. (2022). A review of the application of cerium and lanthanum in phosphorus removal during wastewater treatment: Characteristics, mechanism, and recovery. *Chemosphere*, *309*, 136462.

Kramar, A., Bibik, Y., Dyachenko, A., Chernyayeva, O., Vorobets, V., Kolbasov, G., Smirnova, N., Gaidai, S., Ischenko, O., Eremenko, A., & Linnik, O. (2024). Advanced design of sol-gel derived multilayered cerium titanate films: structural, surface, photoelectrochemical and photocatalytic properties. *Materials Chemistry and Physics*, *324*, 129679.

Lan, Y., Gai, S., Cheng, K., Li, J., & Yang, F. (2022). Lanthanum carbonate hydroxide/magnetite nanoparticles functionalized porous biochar for phosphate adsorption and recovery: Advanced capacity and mechanisms study. *Environmental Research*, *214*, 113783.

Lawrie, G., Keen, I., Drew, B., Chandler-Temple, A., Rintoul, L., Fredericks, P., & Grøndahl, L. (2007). Interactions between Alginate and Chitosan Biopolymers Characterized Using FTIR and XPS. *Biomacromolecules*, *8*(8), 2533–2541.

Li, X., & Cheng, H. (2023). Mn-modified biochars for efficient adsorption and degradation of cephalexin: Insight into the enhanced redox reactivity. *Water Research*, *243*, 120368.

Lin, X., Chen, H., Hu, Z., Hou, Y., & Dai, W. (2018). Enhanced visible light photocatalysis of TiO2 by Co-modification with Eu and Au nanoparticles. *Solid State Sciences*, *83*, 181–187.

Lǚ, J., Liu, H., Liu, R., Zhao, X., Sun, L., & Qu, J. (2013). Adsorptive removal of phosphate by a nanostructured Fe–Al–Mn trimetal oxide adsorbent. *Powder Technology*, *233*, 146–154.

Mishra, A., Ojha, H., Pandey, J., Tiwari, A. K., & Pathak, M. (2023). Adsorption characteristics of magnetized biochar derived from Citrus limetta peels. *Heliyon*, *9*(10), e20665.

Oyekanmi, A. A., Katibi, K. K., Omar, R. C., Ahmad, A., Elbidi, M., Alshammari, M. B., & Shitu, I. G. (2024). A novel oil palm frond magnetic biochar for the efficient adsorption of crystal violet and sunset yellow dyes from aqueous solution: synthesis, kinetics, isotherm, mechanism and reusability studies. *Applied Water Science*, *14*(2), 13.

Peng, H., Gao, P., Chu, G., Pan, B., Peng, J., & Xing, B. (2017). Enhanced adsorption of Cu(II) and Cd(II) by phosphoric acid-modified biochars. *Environmental Pollution*, *229*, 846–853.

Rivera, F. L., Recio, F. J., Palomares, F. J., Sánchez-Marcos, J., Menéndez, N., Mazarío, E., & Herrasti, P. (2020). Fenton-like degradation enhancement of methylene blue dye with magnetic heating induction. *Journal of Electroanalytical Chemistry*, *879*, 114773.

Su, Z., Wang, K., Yang, F., & Zhuang, T. (2023). Antibiotic pollution of the Yellow River in China and its relationship with dissolved organic matter: Distribution and Source identification. *Water Research*, *235*, 119867.

Suo, F., You, X., Yin, S., Wu, H., Zhang, C., Yu, X., Sun, R., & Li, Y. (2021). Preparation and characterization of biochar derived from co-pyrolysis of Enteromorpha prolifera and corn straw and its potential as a soil amendment. *Science of The Total Environment*, *798*, 149167.

Wang, Y., Dong, X., Zang, J., Zhao, X., Jiang, F., Jiang, L., Xiong, C., Wang, N., & Fu, C. (2023). Antibiotic residues of drinking-water and its human exposure risk assessment in rural Eastern China. *Water Research*, *236*, 119940.

Watanabe, S., Tsuda, M., Terada, T., Katsura, T., & Inui, K. (2010). Reduced Renal Clearance of a Zwitterionic Substrate Cephalexin in *Mate1*-Deficient Mice. *Journal of Pharmacology and Experimental Therapeutics*, *334*(2), 651–656.

Supports

Chen, N., Zhao, T., Li, Z., Yue, X., Li, G., Zhang, J., Chen, X., Li, H., Liu, J., Xie, F., Tang, Z., Song, Y., Chen, R., Gan, J., & Li, Y. (2023). Synthesis of ternary Fe-Ca-La oxide composite as highly effective adsorbents to remove phosphate from aqueous solution. *Environmental Technology & Innovation*, *32*, 103326.

Cheng, F., Wang, Y., Fan, Y., Huang, D., Pan, J., & Li, W. (2023). Optimized Ca-Al-La modified biochar with rapid and efficient phosphate removal performance and excellent pH stability. *Arabian Journal of Chemistry*, *16*(8), 104880.

D'Cruz, B., Madkour, M., Amin, M. O., & Al-Hetlani, E. (2020). Efficient and recoverable magnetic AC-Fe$_3$O$_4$ nanocomposite for rapid removal of promazine from wastewater. *Materials Chemistry and Physics*, *240*, 122109.

Fakhri, A., & Adami, S. (2014). Adsorption and thermodynamic study of Cephalosporins antibiotics from aqueous solution onto MgO nanoparticles. *Journal of the Taiwan Institute of Chemical Engineers*, *45*(3), 1001–1006.

Fazal, T., Razzaq, A., Javed, F., Hafeez, A., Rashid, N., Amjad, U. S., Ur Rehman, M. S., Faisal, A., & Rehman, F. (2020). Integrating adsorption and photocatalysis: A cost effective strategy for textile wastewater treatment using hybrid biochar-TiO$_2$ composite. *Journal of Hazardous Materials*, *390*, 121623.

Lu, X., & Zhao, J. (2024). Adsorption of ciprofloxacin on co-pyrolyzed biochar from fish scale and pine needle. *Chinese Journal of Analytical Chemistry*, *52*(1), 100350.

Naghipour, D., Amouei, A., Estaji, M., Taghavi, K., & Allahabadi, A. (2019). Cephalexin adsorption from aqueous solutions by biochar prepared from plantain wood: equilibrium and kinetics studies. *Desalination and water treatment*, *143*, 374–381.

Rashtbari, Y., Hazrati, S., Azari, A., Afshin, S., Fazlzadeh, M., & Vosoughi, M. (2020). A novel, eco-friendly and green synthesis of PPAC-ZnO and PPAC-nZVI nanocomposite using pomegranate peel: Cephalexin adsorption experiments, mechanisms, isotherms and kinetics. *Advanced Powder Technology*, *31*(4), 1612–1623.

Article

Viglašová, E., Galamboš, M., Diviš, D., Danková, Z., Daňo, M., Krivosudský, L., Lengauer, C. L., Matik, M., Briančin, J., & Soja, G. (2020). Engineered biochar as a tool for nitrogen pollutants removal: preparation, characterization and sorption study. *Desalination and water treatment*, *191*, 318–331.

Differences

Ali, I., T. Imanova, G., Alamri, A., Hasan, S. Z., & Basheer, A. A. (2023). Preparation of polyhydroquinone graphene oxide nanocomposite for cephalexin removal from water by adsorption: Simulation, kinetics, and thermodynamic studies. *Inorganic Chemistry Communications*, *157*, 111414.

Fan, X., Qian, Z., Liu, J., Geng, N., Hou, J., & Li, D. (2021). Investigation on the adsorption of antibiotics from water by metal loaded sewage sludge biochar. *Water Science and Technology*, *83*(3), 739–750.

Giannoulia, S., Tekerlekopoulou, A. G., & Aggelopoulos, C. A. (2024). Exploration of cephalexin adsorption mechanisms onto bauxite and palygorskite and regeneration of spent adsorbents with cold plasma bubbling. *Applied Water Science*, *14*(3), 51.

Mangeli, A., Mostafavi, A., Shamspur, T., Fathirad, F., & Mehrabi, F. (2021). Decontamination of fenitrothion from aqueous solutions using rGO/MoS$_2$/Fe$_3$O$_4$ magnetic nanosorbent: synthesis, characterization and removal application. *Journal of Environmental Health Science and Engineering*, *19*(2), 1505–1511.

Nawaz, H., Ibrahim, M., Mahmood, A., Kotchey, G. P., & Sanchez, D. V. P. (2023). An efficient synthesis and characterization of La@MOF-808: A promising strategy for effective arsenic ion removal from water. *Heliyon*, *9*(11), e21572.

Puga, A., Moreira, M. M., Pazos, M., Figueiredo, S. A., Sanromán, M. Á., Delerue-Matos, C., & Rosales, E. (2022). Continuous adsorption studies of pharmaceuticals in multicomponent mixtures by agroforestry biochar. *Journal of Environmental Chemical Engineering*, *10*(1), 106977.

Rashtbari, Y., Hazrati, S., Afshin, S., Fazlzadeh, M., & Vosoughi, M. (2018). Data on cephalexin removal using powdered activated carbon (PPAC) derived from pomegranate peel. *Data in Brief*, *20*, 1434–1439.

Wang, H.-Y., Kumar, A., Li, J., Chen, P., Yu, Z.-G., & Sun, G.-X. (2023). The adsorption behavior and mechanism for arsenate by lanthanum-loaded biochar with different modification methods. *Environmental Technology & Innovation*, *32*, 103344.

Yaghini, M., & Faghihian, H. (2020). Novel magnetized carbon core-shell impregnated with lanthanum as an adsorbent for uptake of fluoride from aquatic systems, studied by response surface methodology. *Desalination and Water Treatment*, *179*, 160–171.

Discussions

Acelas, N., Lopera, S. M., Porras, J., & Torres-Palma, R. A. (2021). Evaluating the Removal of the Antibiotic Cephalexin from Aqueous Solutions Using an Adsorbent Obtained from Palm Oil Fiber. *Molecules*, *26*(11), 3340.

Gao, Y., He, D., Wu, L., Wang, Z., Yao, Y., Huang, Z.-H., Yang, H., & Wang, M.-X. (2020). Porous and ultrafine nitrogen-doped carbon nanofibers from bacterial cellulose with superior adsorption capacity for adsorption removal of low-concentration 4-chlorophenol. *Chemical Engineering Journal*, 127411.

Groeneveld, I., Kanelli, M., Ariese, F., & van Bommel, M. R. (2023). Parameters that affect the photodegradation of dyes and pigments in solution and on substrate – An overview. *Dyes and Pigments*, *210*, 110999.

Imanipoor, J., Ghafelebashi, A., Mohammadi, M., Dinari, M., & Ehsani, M. R. (2021). Fast and effective adsorption of amoxicillin from aqueous solutions by L-methionine modified montmorillonite K10. *Colloids and Surfaces A: Physicochemical and Engineering Aspects*, *611*, 125792.

Karlsson, J. K. G., Woodford, O. J., Al-Aqar, R., & Harriman, A. (2017). Effects of Temperature and Concentration on the Rate of Photobleaching of Erythrosine in Water. *The Journal of Physical Chemistry A*, *121*(45), 8569–8576.

Kaya, N., & Uzun, Z. Y. (2024). Experimental and modeling studies on the removal of bromocresol green from aqueous solutions by using pine cone-derived activated biochar. *Biomass Conversion and Biorefinery*.

Krasucka, P., Pan, B., Sik Ok, Y., Mohan, D., Sarkar, B., & Oleszczuk, P. (2021). Engineered biochar – A sustainable solution for the removal of antibiotics from water. *Chemical Engineering Journal*, *405*, 126926.

Masulli, M., Liu, Z.-L., Guo, F.-Z., Li, X., Sudhölter, E. J. R., & Kumar, N. (2022). Temperature effect on the dynamic adsorption of anionic surfactants and alkalis to silica surfaces. *Petroleum Science*, *19*(4), 1866–1876.

Moreroa-Monyelo, M., Falayi, T., Ntuli, F., & Magwa, N. (2022). Studies towards the adsorption of sulphate ions from acid mine drainage by modified attapulgite clays. *South African Journal of Chemical Engineering*, *42*, 241–254.

Ndoun, M. C., Elliott, H. A., Preisendanz, H. E., Williams, C. F., Knopf, A., & Watson, J. E. (2021). Adsorption of pharmaceuticals from aqueous solutions using biochar derived from cotton gin waste and guayule bagasse. *Biochar*, *3*(1), 89–104.

Wernke, G., Shimabuku-Biadola, Q. L., dos Santos, T. R. T., Silva, M. F., Fagundes-Klen, M. R., & Bergamasco, R. (2020). Adsorption of cephalexin in aqueous media by graphene oxide: kinetics, isotherm, and thermodynamics. *Environmental Science and Pollution Research*, *27*(5), 4725–4736.

Wong, Y. C., Szeto, Y. S., Cheung, W. H., & McKay, G. (2008). Effect of temperature, particle size and percentage deacetylation on the adsorption of acid dyes on chitosan. *Adsorption*, *14*(1), 11–20.

Electromagnetic theory: Electromagnetic pulse in the laboratory

Teoría electromagnética: Pulso electromagnético en el laboratorio

Guzmán-Tinajero, Pedro* [a], Hernández-Gómez, Víctor Hugo [b] and Castro-Fuentes, Aide [c]

[a] ROR Facultad de Estudios Superiores Cuautitlán UNAM • ACR-9145-2022 • 0000-0002-2297-7758 • 251228
[b] ROR Facultad de Estudios Superiores Cuautitlán UNAM • S-6575-2018 • 0000-0001-9315-5869 • 122247
[c] ROR Facultad de Estudios Superiores Cuautitlán UNAM • LCD-6923-2024 • 0009-0006-7406-8579 • 2059588

Abstract

This article shows the process in the development of a laboratory practice of Electromagnetic Theory, applied to the Telecommunications, Systems and Electronics Engineering Career, of the Facultad de Estudios Superiores Cuautitlán (FESC) belonging to the Universidad Nacional Autónoma de México (UNAM). The objective for future engineers is to learn about the impact of an electromagnetic pulse on electronic equipment. It begins with the theoretical background of the electromagnetic pulse, then basic oscillator circuits are addressed and an experiment with a low-power electromagnetic pulse is developed. The impact of the practice on the students is measured and with it, conclusions are drawn, indicating the importance of this knowledge for future engineers in telecommunications systems and electronics.

Resumen

En este artículo se muestra el proceso en el desarrollo de una práctica de laboratorio de Teoría Electromagnética, aplicado a la Carrera de Ingeniero en Telecomunicaciones Sistemas y Electrónica, de la Facultad de Estudios Superiores Cuautitlán (FESC) perteneciente a la Universidad Nacional Autónoma de México (UNAM). El objetivo para los futuros ingenieros es conocer el impacto de un pulso electromagnético en los equipos electrónicos. Se comienza por los antecedentes teóricos del pulso electromagnético, posteriormente se abordan los circuitos osciladores básicos y se desarrolla un experimento con un pulso electromagnético de baja potencia. Se mide el impacto de la práctica en los alumnos y con ello, se establecen las conclusiones, indicando la importancia de este conocimiento para los futuros ingenieros en telecomunicaciones sistemas y electrónica.

Electromagnetic Theory: Electromagnetic Pulse in the laboratory
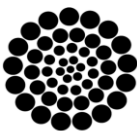
Objective	Background	Conclusions
Produce and apply a low power electromagnetic pulse.	EM Waves, The Van De Graaff Generator	It has a beneficial impact on teachers and students.
Methodology	Results	Contributions
Circuit, EMP	Theoretical and practical knowledge	Improved learning
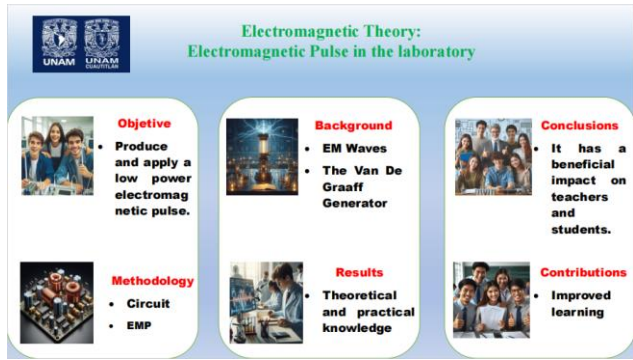
Telecommunications, Laboratory, Pulse

Teoría Electromagnética: Pulso Electromagnético en el laboratorio

Objetivo	Antecedentes	Conclusiones
Producir y aplicar un pulso electromagnético de baja potencia.	Ondas TEM, Generador Van De Graaff	Tiene un impacto beneficioso en profesores y alumnos
Metodología	Resultados	Contribuciones
Circuito, PEM	Conocimiento teórico y práctico	Mejora del aprendizaje

Telecomunicaciones, Laboratorio, Pulso

RENIECYT
Registro Nacional de Instituciones y Empresas Científicas y Tecnológicas
1702902 CONAHCYT

Article

Introducción

The Facultad de Estudios Superiores Cuautitlán (FESC), part of the Universidad Nacional Autónoma de México (UNAM), is an important academic center located in the municipality of Cuautitlán Izcalli, State of Mexico. It was inaugurated on April 22, 1974, and has been in existence for more than 50 years. It now has 17 degree programs and has approximately 18,000 students enrolled.

In the curriculum of the Telecommunications Systems and Electronics Engineer (ITSE), taught at the FESC of the UNAM is the subject of Electromagnetic Theory, located in the fifth semester of the career and marked as a theoretical and practical subject (therefore includes a laboratory), has 10 mandatory credits, so it is of great importance in the training of future engineers.

According to Yeang (2024), Electromagnetism and electrodynamics, central to classical physics, began with Ampère's electrodynamics and Faraday's electromagnetic induction. By the mid-19th century, Neumann and Weber developed a unified electrical theory, while Faraday and Thomson explored the electromagnetic field. Maxwell expanded this theory, introducing the displacement current and predicting electromagnetic waves, which Helmholtz further developed, leading to Hertz's 1887 discovery of electric waves.

In the internal structure of the Electromagnetic theory subject, the topic of "Fundamentals of Electrodynamics" is located, and within it, subtopics such as Maxwell's Equations, electric potential and Gauss's Law among others. Source: FESC (2024).

Within the Electromagnetic Theory, the Electromagnetic Pulse, also referred to in the literature as EMP, is a phenomenon that has gained increasing relevance, due to its high impact on electronic devices and communication systems, increasingly used by our students in Universities.

The EMP is defined as a rapid release of electromagnetic energy, generating waves that can affect electronic systems through the induction of currents and voltages.

Its importance lies in the vulnerability of modern infrastructure to these pulses, since critical devices, such as power and communication systems, may suffer irreparable damage.

According to Mendieta (2008), in the 1940s, after experimenting with the first Atomic Bomb, very destructive effects were observed in electrical and electronic devices on the Island of Hawaii, and as tests continued and the destructive effect of these was observed, the "Comprehensive Nuclear Test Ban Treaty" (CTBT) was proposed.

For the scope of this article, we will focus on Electromagnetic Pulses generated in the laboratory through voltage variations such as those produced by the Van De Graaff Generator.

The problem we wanted to attack was the general ignorance of our students to the EMP phenomenon and the importance that it has in the proper functioning of electronic devices today.

The contribution of this experiment is the realization of a controlled EMP, as well as the design and measurement of the basic circuit to raise the voltage, all this is visually attractive to students and motivates them the deepen of the subject.

For all of the above, we developed a laboratory practice called: "Passive circuits and electromagnetic pulse", which has already been included in the manual of laboratory practices of the Physics Department of the FESC UNAM.

The results were encouraging, especially improving the interest of our students in Electromagnetic Theory. It should be noted that these young people will be the future engineers in telecommunications, systems, and electronics of the Universidad Nacional Autónoma de México (UNAM).

Methodology

For the elaboration of this work, first a theoretical research was carried out that included basic elements of the Electromagnetic Theory subject, the programmatic contents approved by the H. Technical Council of the Faculty, and the quality guidelines according to the ISO 9001:2015 standard were considered.

We worked with several academics belonging to the Electromagnetic Theory faculty to distribute the work equitably.

Considering that Maxwell's equations refer to the conversion of electric and magnetic fields, we decided to include an experiment that had the necessary characteristics to make it attractive to students and at the same time demonstrate the relationship between the mentioned fields.

All the topics of the theoretical course were covered and several practices were developed, all of which resulted in the laboratory practices manual.

For this article, only practice 3, called Passive Circuits and Electromagnetic Pulse, was considered. This practice was first applied in a pilot test to teachers and students, with the feedback obtained, modifications were made and the final product was obtained, which was integrated to the Laboratory Manual and sent to the Physics Department for its electronic publication.

Van De Graaff Generator and Electromagnetic Theory

Within the theoretical analysis, a review of Maxwell's equations, RC (Resistive-Capacitive), RL (Resistive-Inductive), CL (Capacitive-Inductive), and RCL (Resistive-Capacitive-Inductive) circuits, as well as a historical review of the PEM starting with Robert J. Van de Graaff were considered.

According to Open AI (2022), in 1929, Robert J. Van de Graaff, a graduate student at the Massachusetts Institute of Technology (MIT), decided to build what would become the first Van de Graaff generator.

The original Van de Graaff Generator is a device that, through a moving conveyor belt, accumulates electric charge in a hollow metal sphere. Its primary purpose was to generate exceptionally high electrical voltages to undertake research into the dispersion of charged particles.

Over the years Van de Graaf's initial design has been modified to the equipment we have in our laboratories.

Where not all the bands (made of latex) present friction with the hull of the Generator, instead they induce the charges on it. There are even some generators where the mechanical movement has been replaced by a voltage booster circuit, also known as boost converter.

Development of the Experiment

For this project we used the Van De Graaff Generator of the Physics Laboratory, FESC, which works with the friction of the band on a roller and the induction of charges to the generator shell, see Figure 1, to produce a controlled EMP that allowed the students enrolled in the Electromagnetic Theory course to observe the effect of the same on electronic devices.

Box 1

Figure 1

Van De Graff generator

Source: Own Elaboration

Compared to other techniques (such as nuclear), the PEM generated by the Van De Graaff Generator is of low power, which allows students to understand and measure it more safely.

We also built a passive oscillator circuit with laboratory elements (Capacitive-Inductive circuit) and accompanied it with a Diode to produce the effect of voltage growth in the capacitor. See Figure 2
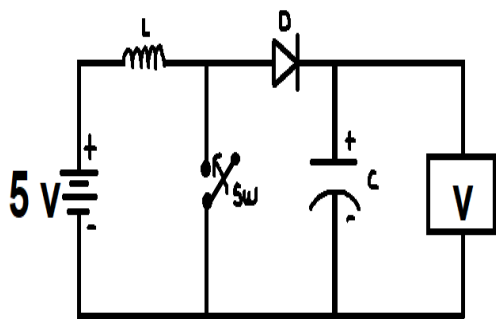
Guzmán-Tinajero, Pedro, Hernández-Gómez, Víctor Hugo and Castro-Fuentes, Aide. [2024]. Electromagnetic theory: Electromagnetic pulse in the laboratory. Journal of Systematic Innovation. 8[22]1-7: e3822107.
https://doi.org/10.35429/JSI.2024.8.22.3.7

Box 2

Figure 2

Wiring diagram

Source: Own Elaboration

We consider it important to mention that, although we could have worked with a power transistor, to make the experiment more didactic we used a basic button switch.

By using the basic switch, we were able to allow the students to interact with the circuit and demonstrate the relevance of the operating frequency in a practical and didactic way.

Elaboration of the laboratory practice

The Laboratory of the Physics Department of the FESC is certified under the ISO 9001-2015 standard, which is why when introducing a new practice it was necessary to comply with certain organizational guidelines.

According to Departamento de Física (2024), the structure of each of the practices of the manual for the Electromagnetic Theory laboratory, consists of 8 main elements, see Table 1.

Box 3

Table 1

Structure of the practice

1.	Home page
2.	Previous knowledge
3.	Objectives
4.	Theoretical foundations
5.	Previous questionnaire
6.	Materials and equipment
7.	Development
8.	Conclusions

Source: Own Elaboration

The proposed practice complied with these guidelines and additionally, being a product of a collegiate work, it could be integrated to a UNAM program called: Program of Support to Projects for the Innovation and Improvement of Teaching (PAPIME for its acronym in Spanish), which indicated additional elements to be considered, which was fulfilled in the drafting determining the final structure of the document.

The final work consisted of 15 pages, including the cover page. Its name was: Practice 3. Passive circuits and electromagnetic pulse. It was presented to a pilot group of teachers for their observations and later to a pilot group of students to evaluate its impact.

Box 4
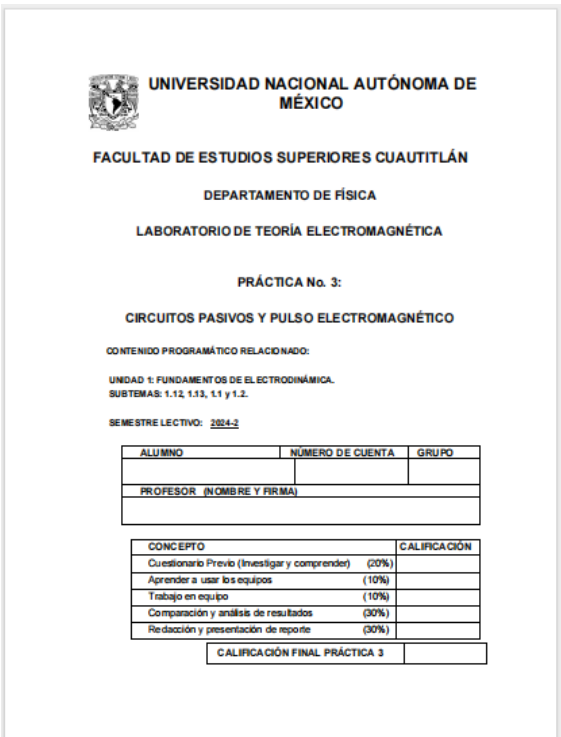
Figure 3

Cover page of the practice

Source: Own Elaboration

For the electromagnetic pulse part, the Van de Graff and a basic calculator were added, the students were asked to place a certain level of band velocity to generate sufficient charge and then at different distances to measure the impact of the electric field on the electronic device. As can be seen in Figure 4.

Guzmán-Tinajero, Pedro, Hernández-Gómez, Víctor Hugo and Castro-Fuentes, Aide. [2024]. Electromagnetic theory: Electromagnetic pulse in the laboratory. Journal of Systematic Innovation. 8[22]1-7: e3822107. https://doi.org/10.35429/JSI.2024.8.22.3.7

Box 5
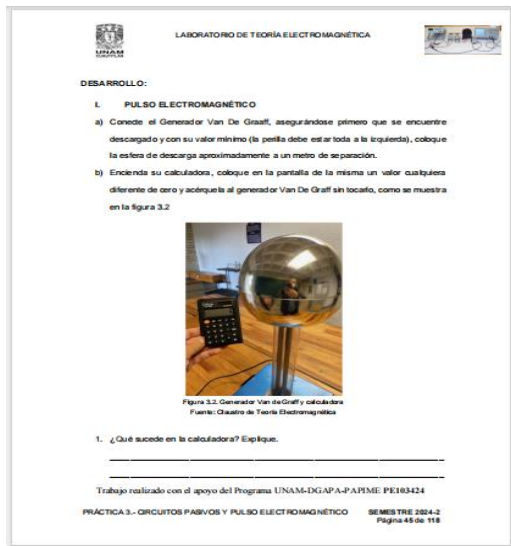
Figure 4

Electromagnetic Pulse Experiment

Source: Own Elaboration

The experiment with the voltage booster circuit was also developed with safety measures in mind, including the use of an acrylic enclosure to prevent incidents with the capacitor and to protect the students. See Figure 5.

Box 6
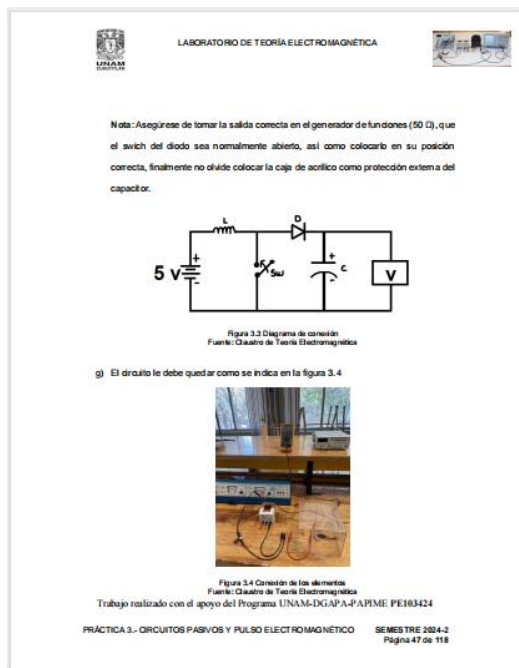
Figure 5

Experiment developing the circuit

Source: Own Elaboration

Students were asked to take different readings and interact with the switch at various speeds to observe the effect of frequency on these circuits.

Results

During the development of the study, a significant understanding on the part of the students concerning the concept of electromagnetic pulse was observed.

This finding suggests a deep understanding on the part of the students about this phenomenon, which indicates remarkable progress in their learning.

In addition, the teachers participating in the study were able to develop and strengthen their didactic skills by incorporating new tools and strategies to improve the teaching of the Electromagnetic Theory course.

This pedagogical adaptation can be considered an important achievement for the teaching team, as it allows them to offer a more enriching and effective educational experience to their students.

Regarding the students' understanding of the operation of a voltage booster circuit, the results showed a satisfactory level of comprehension. This ability acquired by the students suggests an improvement in their knowledge and skills in the field of electronics and telecommunications engineering.

In general, the objectives set for the practical were achieved, which included:

- To observe phenomena related to electric charges in motion, interacting with electric and magnetic fields, through passive circuits.

- To produce and apply a low-power electromagnetic pulse.

These results confirm the effectiveness of the methodological approach used in practice, as well as the students' ability to assimilate and apply the theoretical concepts learned in a practical context.

Conclusions

The results obtained in this study provide a clear view of the positive impact that the lab session had on students' learning and the professional development of teachers. From these findings, several important conclusions can be drawn:

Guzmán-Tinajero, Pedro, Hernández-Gómez, Víctor Hugo and Castro-Fuentes, Aide. [2024]. Electromagnetic theory: Electromagnetic pulse in the laboratory. Journal of Systematic Innovation. 8[22]1-7: e3822107.
https://doi.org/10.35429/JSI.2024.8.22.3.7

Effectiveness of the pedagogical approach: The lab session was effective in enhancing students' understanding of fundamental electromagnetics and electrical circuit concepts. The integration of theory with hands-on practice enabled a deeper and more meaningful comprehension of the studied phenomena.

Teacher development: The results indicate that the participating teachers were able to strengthen their didactic skills and adapt their pedagogical approach to offer a more enriching learning experience. This aspect is crucial to improve the quality of teaching and learning in the classroom.

Practical application of knowledge: Practice allowed students not only to understand theoretical concepts, but also to apply them in practical situations. This is essential for developing practical skills and fostering critical and creative thinking in students.

Fulfillment of objectives: It was confirmed that the objectives set for the practicum were satisfactorily achieved. Students were able to observe and apply electromagnetic phenomena, while teachers were able to strengthen their course with new tools and approaches.

In summary, the results highlight the importance of educational practices based on experience and active interaction with content, both for students' learning and for teachers' professional development. These findings can serve as a basis for future research and the continuous improvement of academic programs and teaching in general.

Declarations

Conflict of interest

The authors declare no interest conflict. They have no known competing financial interests or personal relationships that could have appeared to influence the article reported in this article.

Authors' Contribution

The contribution of each researcher in each of the points developed in this research, was defined based on:

Guzmán-Tinajero, Pedro: Contributed to the project idea, research method, and technique. He supported the design of the field instrument. He carried out the data analysis and systematization of results, as well as writing the article.

Hernández-Gómez, Víctor Hugo: Carried out the systematisation of the background for the state of the art. She supported the design of the field instrument. She also contributed to the writing of the article.

Castro-Fuentes, Aide: contributed to the research design, the type of research, the approach, the method, and the writing of the article.

Availability of data and materials

The images were obtained from photographs taken at the physics laboratory of the Facultad de Estudios Superiores Cuautitlán, UNAM.

Acknowledgments

Funding

Abbreviations

CTBT	Comprehensive Nuclear Test Ban Treaty
EMP	Electromagnetic Pulse
FESC	Eaculty of Higher Studies Cuautitlán
ISO	Internacional Organization for Standardization
ITSE	Telecommunications Engineering Systems and Electronics
MIT	Massachusetts Institute of Technology

Guzmán-Tinajero, Pedro, Hernández-Gómez, Víctor Hugo and Castro-Fuentes, Aide. [2024]. Electromagnetic theory: Electromagnetic pulse in the laboratory. Journal of Systematic Innovation. 8[22]1-7: e3822107.
https://doi.org/10.35429/JSI.2024.8.22.3.7

PAPIME	Program of Support to Projects for the Innovation and Improvement of Teaching
RC	Resistive Capacitive
RCL	Resistive Capacitive Inductive
RL	Resistive Inductive

References

Basics

Yeang, C.-P. (2024). Electromagnetism and electrodynamics in the 19th century. In B. Foster et al. (Eds.), Oxford research encyclopedia of physics (Article ID 131). Oxford University Press and the American Institute of Physics.

FESC (2024). "Syllabus of the Electromagnetic Theory subject."

Mendieta, J. (2008). "The Electromagnetic Pulse (EMP): The Most Destructive Energy." Universidad Politécnica Salesiana. Spain.

OpenAI. (2022). "Who was Van de Graaff?" OpenAI GPT-3.5.:

Supports

Departamento de Física (2024). " Práctica de Teoría Electromagnética: Circuitos pasivos y pulso electromagnético"

Influence of concentration, acid type and calcination temperature on TiO₂ synthesis

Influencia de la concentración, el tipo de ácido y la temperatura de calcinación en la síntesis de TiO₂

Del Ángel-Sánchez, María Magdalena [a] & Martínez-Carreón, María de Jesús *[b]

[a] ROR Universidad Tecnológica Gral. Mariano Escobedo • LDG-8077-2024 • 0009-0002-9241-5117 • 416112
[b] ROR Universidad Autónoma de Nuevo León • IYJ-9475-2023 • 0000-0002-9283-7857 • 290939
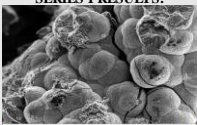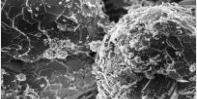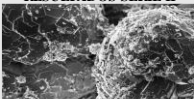
Abstract

Titanium dioxide (TiO₂) is employed in various environmental science applications due to its exceptional photocatalytic activity and semiconductor behavior. The efficacy of TiO₂ in these applications is intrinsically linked to its crystal structure, morphology and particle size. Titanium dioxide exhibits three well-defined crystalline phases: Anatase (octahedral structure), Rutile (tetragonal structure) and Brookite (orthorhombic structure). This work studies the effect of different concentrations, types of acids, and calcination temperatures on the crystalline structure and morphology of TiO₂ synthesized via hydrothermal route using characterization techniques such as DLS (Dynamic Light Scattering), ATR-FTIR (Attenuated Total Reflectance Fourier Transform Infrared Spectroscopy), XRD (X-Ray Diffraction) and SEM (Scanning Electron Microscopy).

Resumen

El dióxido de titanio (TiO₂) se emplea en diversas aplicaciones de ciencia ambiental debido a su excepcional actividad fotocatalítica y su comportamiento como semiconductor, La eficacia del TiO₂ en estas aplicaciones está intrínsecamente ligada a su estructura cristalina, morfología y tamaño de partícula. El TiO₂ presenta tres fases cristalinas bien definidas: Anatasa (estructura octaédrica), Rutilo (estructura tetragonal) y Brookita (estructura ortorrómbica). En este trabajo se estudia el efecto de diferentes concentraciones, tipos de ácidos y temperatura de calcinación en la estructura cristalina y morfología del TiO₂ sintetizado por vía hidrotermal mediante las técnicas de caracterización de dispersión de luz dinámica (DLS), espectroscopia infrarroja por transformada de Fourier con reflectancia total atenuada (ATR-FTIR), difracción de rayos X (XRD) y microscopía electrónica de barrido (SEM).

Influence of concentration, acid type and calcination temperature on TiO₂ synthesis

OBJECTIVE:	SERIES I METHODOLOGY:						SERIES I RESULTS:
Study the effect of different concentrations, types of acids, and calcination temperature on the crystalline structure and morphology of TiO₂ via hydrothermal method; In Series I varying the percentage of nitric acid and in Series II varying the ratio of HCl:HNO₃	REACTANT	SAMPLE					
		I-1	I-2	I-3	I-4	I-5	
	HNO₃	0M	1M	3M	1M	0.5M	
	Ti i(PrO)₄	0.15M	0.15M	0.15M	0.15M	0.15M	
	NaF	-	-	-	0.01M	-	

SERIES II METHODOLOGY:				SERIES II RESULTS:
REACTANT	SAMPLE			
	II-1	II-2	II-3	
HNO₃	0.5M	1M	1.5M	
HCl	2.5M	2M	1.5M	
Ti i(PrO)₄	0.15M	0.15M	0.15M	

Influencia de la concentración, el tipo de ácido y la temperatura de calcinación en la síntesis de TiO₂

OBJETIVO:	METODOLOGÍA SERIE I:						RESULTADOS SERIE I:
Estudiar el efecto de diferentes concentraciones, tipos de ácidos y temperatura de calcinación en la estructura cristalina y morfología del TiO₂ por vía hidrotermal; En la síntesis I variando el porcentaje de ácido nítrico y en la Serie II variando la relación de HCl:HNO₃	REACTIVO	MUESTRA					
		I-1	I-2	I-3	I-4	I-5	
	HNO₃	0M	1M	3M	1M	0.5M	
	Ti i(PrO)₄	0.15M	0.15M	0.15M	0.15M	0.15M	
	NaF	-	-	-	0.01M	-	

METODOLOGÍA SERIE II:				RESULTADOS SERIE II
REACTIVO	MUESTRA			
	II-1	II-2	II-3	
HNO₃	0.5M	1M	1.5M	
HCl	2.5M	2M	1.5M	
Ti i(PrO)₄	0.15M	0.15M	0.15M	

Titanium dioxide TiO₂, Hydrothermal synthesis, Structural analysis.

Dióxido de titanio TiO₂, Síntesis hidrotermal, Análisis estructural

RENIECYT
Registro Nacional de Instituciones y Empresas Científicas y Tecnológicas
1702902 CONAHCYT

Article

Introduction

Titania has a wide range of applications in environmental science due to its excellent catalytic, optical and electrical properties (Farooq, 2024). It is frequently used for the photodegradation of organic molecules, water purification, disinfection of wastewater, self-cleaning coatings for buildings in urban areas and in water splitting for hydrogen generation (Ali, 2018). Additionally, exhibits utility in air remediation systems, disinfection processes, and targeted organic transformations (Arun, 2023). These applications highlight the importance of TiO$_2$ in addressing environmental challenges and promoting sustainability (Pelaez, 2012).

Numerous methodologies have been developed for the synthesis of titanium dioxide, encompassing techniques such as hydrothermal synthesis (Hidalgo, 2007), metal-organic chemical vapor deposition (MOCVD) (Li, 2002), electrochemical approaches (Anandgaonker, 2019), sonochemical processes (Guo, 2011), and green synthesis routes (Dülger, 2024), among others.

Hydrothermal synthesis of TiO$_2$ nanoparticles was performed. This method typically involves the crystallization of TiO$_2$ from a precursor solution under high pressure and temperature conditions. The hydrothermal process can produce either rutile or anatase phase nanoparticles depending on the specific conditions and precursors used (Gupta, 2021), (Rehan, 2011). The influence of reactant concentration and acid type on the final properties of TiO$_2$ nanoparticles synthesized via hydrothermal methods is an important area of research for evaluating the impact of key reaction parameters on their crystallinity (Kignelman, 2021).

Precursor concentration is known to significantly impact the size, morphology, and crystallinity of the resulting nanostructures (Bindra, 2022), (Huang, 2012), these factors directly influence the catalytic efficiency and potential applications of TiO$_2$. Similarly, the type of acid employed dictates the etching behavior during synthesis, thereby affecting the final morphology and size of the nanostructures (Eaimsumang, 2020). A thorough understanding of these influences allows for the targeted design and optimization of TiO$_2$ for specific applications.

In the present investigation, the effects of nitric acid (HNO$_3$) concentration gradients and calcination temperature on the hydrothermal fabrication of titanium dioxide are elucidated. Furthermore, this work delineates the comparative impact of acid type on TiO$_2$ synthesis by utilizing both HNO$_3$ and hydrochloric acid (HCl) across a spectrum of concentrations and thermal conditions.

Materials and methods

Two series of syntheses were conducted. In series I, different concentrations of nitric acid and two distinct calcination temperatures were utilized, whereas in series II, molar ratios of nitric acid to hydrochloric acid were employed.

Series I: Synthesis of titania particles was achieved utilizing titanium isopropoxide (Ti i(PrO)$_4$) as the precursor. This precursor was incrementally introduced, via a dropwise method, into diverse solutions of nitric acid (HNO$_3$), accompanied by continuous stirring for a duration of 30 minutes at ambient temperature. To one synthesis batch, sodium fluoride (NaF) was incorporated to evaluate its effect, given that the fluoride ion (F$^-$) demonstrates a pronounced complexation propensity towards Ti(IV). The specific compositions for each solution are enumerated in Table No. 1.

After the completion of the stirring phase, all synthetic mixtures were transferred to hermetically sealed polyethylene containers and subjected to an aging process at 85°C within an oven for a period of 24 hours. Post-aging, selected sample aliquots underwent calcination at temperatures of 300°C and 500°C. The residual precipitates were subjected to centrifugation at 8000 rpm for 10 minutes followed by washing. The precipitates that resulted from this process were then calcined at a temperature of 300°C.

Box 1

Table 1

Reactant Concentrations for Titanium Dioxide Synthesis in Series I

Reactant	Sample				
	I-1	I-2	I-3	I-4	I-5
HNO$_3$	0M	1M	3M	1M	0.5M
Ti i(PrO)$_4$	0.15M	0.15M	0.15M	0.15M	0.15M
NaF	-	-	-	0.01M	-

Source: own elaboration

Series II: Titanium dioxide was synthesized by introducing titanium isopropoxide into a variety of HCl and HNO$_3$ solutions, maintaining an aggregate acid concentration of 3M while varying their respective proportions. The synthesis proceeded under continuous stirring for 30 minutes. The final concentrations are enumerated in Table No. 2.

Subsequently, the samples underwent an aging process for 24 hours at 85°C within a controlled oven environment. Post-aging, the samples were subjected to centrifugation, and the resultant solid was rinsed and re-centrifuged at 8000 rpm for a duration of 5 minutes. The solid isolated from this stage was then redissolved in 50 mL of 3M HNO$_3$ with stirring maintained for 20 minutes. Following this, the samples were once again centrifuged and washed; the solid fraction was segregated from the supernatant and subsequently desiccated.

Box 2

Table 2

Reactant Concentrations for Titanium Dioxide Synthesis in Series II

Reactant	Sample		
	II-1	II-2	II-3
HNO$_3$	0.5M	1M	1.5M
HCl	2.5M	2M	1.5M
Ti i(PrO)$_4$	0.15M	0.15M	0.15M

The suspensions derived post-centrifugation in series I were subjected to particle size analysis utilizing a Dynamic Light Scattering (DLS) device NanoBrook 90Plus Particle Size Analyzer (Brookhaven Instruments Corporation).

The two series of samples were characterized by XRD using a PANalytical X'Pert PRO diffractometer operated at 40kV and 40mA, employing Cu-Kα radiation (λ= 1.54060Å) with a step size of 0.0260° and a counting time of 1.0s per step.

The presence of functional groups was determined using a Shimadzu IRAffinity FTIR instrument, equipped with a Gladi ATR module (PIKE Technologies, INC) with a spectral range of 500 to 4000 cm^{-1}.

The morphology of the materials was determined using Field Emission Scanning Electron Microscopy (FESEM) on a Carl Zeiss Supra 40 NTS instrument.

Results and discussions

Characterization by DLS

The soles obtained from samples I-2, I-4, and I-5 were characterized. Samples I-1 and I-3 could not be peptized due to consecutive washing of the solid obtained by thermal hydrolysis.

Figures 1 to 3 display the histograms corresponding to the different samples. In sample I-2, a particle size of 220 nm with a polydispersity index of 0.261 was obtained, sample I-4 has a particle size of 167 nm with a polydispersity index of 0.278, while in sample I-5, the particle size is 1291 nm with a polydispersity index of 0.005. In syntheses I-2 and I-4, higher acid concentrations were used compared with sample I-5, which generated smaller particles resulting in a more stable sol. Sample I-5, containing a lower concentration of HNO$_3$, produced an unstable sol that formed a precipitate after 30 minutes.

Box 3
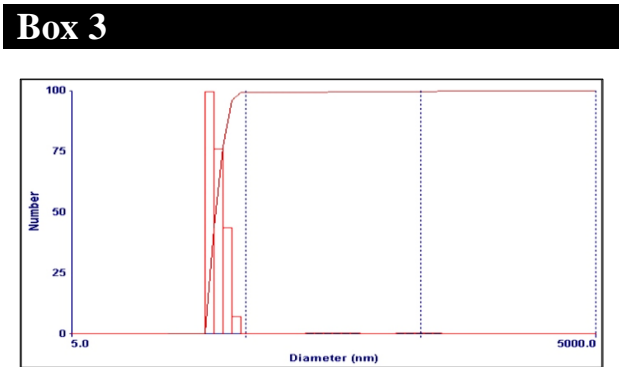
Figure 1

DLS size distribution of sample I-2
Source: 90Plus Nanoparticle Size Analyzer

Box 4
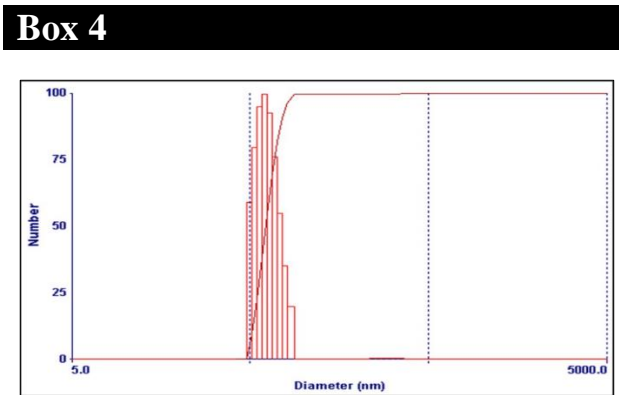
Figure 2

DLS size distribution of sample I-4
Source: 90Plus Nanoparticle Size Analyzer

Box 5
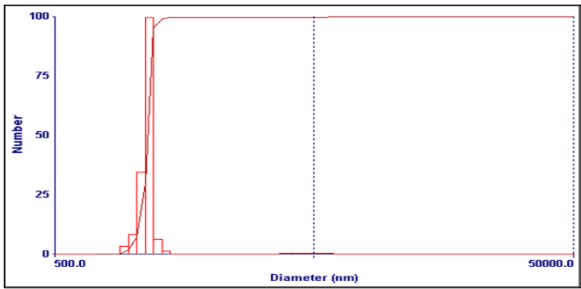
Figure 3

DLS size distribution of sample I-5
Source: 90Plus Nanoparticle Size Analyzer

Characterization by XRD

The samples from series I, subjected to calcination at 300°C, were analyzed using X-ray diffraction (XRD). In Figure 4, it is evident that samples I-2 and I-5 exhibit the crystalline phase of anatase, as indicated by the International Centre for Diffraction Data (ICDD) card 00-004-0477. Conversely, the crystalline phase of sample I-3 corresponds to rutile, matching with the information linked to the ICDD 01-073-1765 card.

Box 6
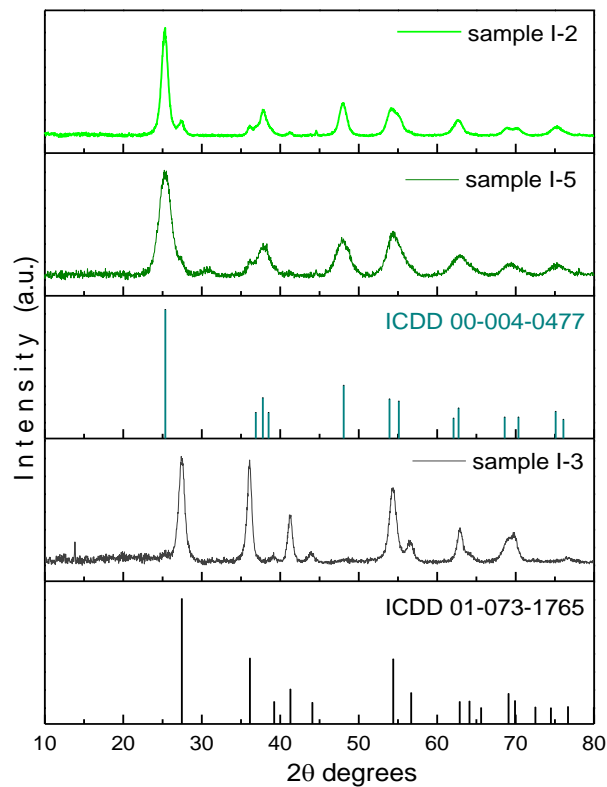
Figure 4

X-ray diffraction patterns of Series I samples calcined at 300°C

Source: Own elaboration

The average crystallite sizes of the samples presented in Table 3 were determined using the Scherrer equation, analyzing the diffraction peaks with the X'Pert HighScore Plus software.

Box 7

Table 3

Crystallite Size of Series I Samples Calcined at 300°

Sample	Crystallite size [Å]
I-2	81.5
I-3	108.2
I-5	41.6

Source: own elaboration

XRD analysis was performed on Series I samples calcined at 500°C. The corresponding diffractograms are presented in Figure 5. Consistent with the observations for samples calcined at 300°C, samples I-2 and I-5 exhibit the anatase crystalline phase, as evidenced by their diffraction patterns matching the ICDD card 00-004-0477. In contrast, sample I-3 possesses a rutile crystalline phase, as confirmed by its diffraction pattern aligning with the ICDD card 01-073-1765.

Box 8
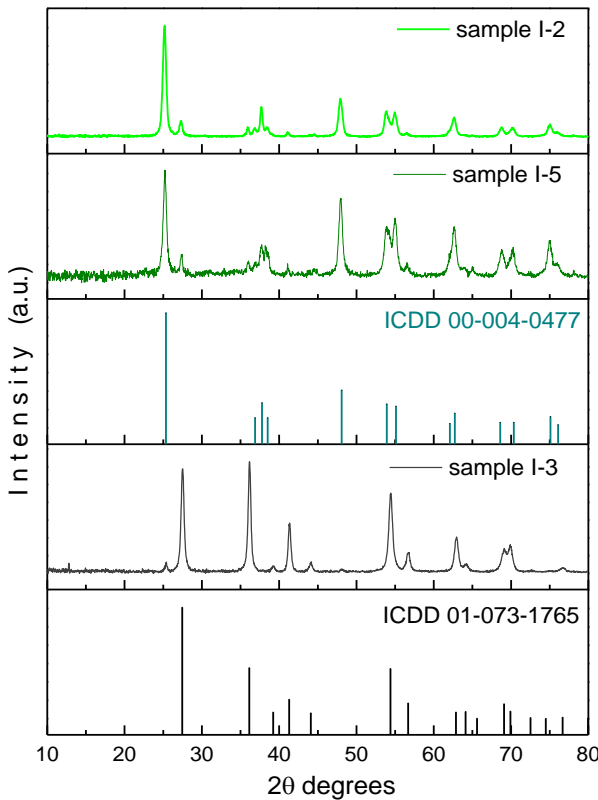
Figure 5

X-ray diffraction patterns of Series I samples calcined at 500°C

Source: Own elaboration

Del Ángel-Sánchez, María Magdalena & Martínez-Carreón, María de Jesús. [2024]. Influence of concentration, acid type and calcination temperature on TiO₂ synthesis. Journal of Systematic Innovation. 8[22]1-11: e4822111.
https://doi.org/10.35429/JSI.2024.8.22.1.11

Journal of Systematic Innovation

Article

Crystallite size was determined by analyzing the diffraction peaks of Figure 5 using the Scherrer equation within X'Pert HighScore Plus software. The results are presented in Table 4.

Box 9

Table 4

Crystallite Size of Series I Samples Calcined at 500°

Sample	Crystallite size [Å]
I-2	170.9
I-3	182.5
I-5	161.5

Source: own elaboration

In the syntheses of Series I, it is evident that as the precursor solution is prepared in a more acidic medium, the development of the rutile phase is favored (sample I-3), in contrast to samples synthesized in a less acidic medium (samples I-2 and I-5), where characteristic peaks corresponding to the anatase phase are observed.

Regarding the calcination temperature, examination of the diffractograms in figures 4 and 5 reveals that there is no change in the samples with respect to the phases present. However, the thermal treatment led to an increase in crystal size, as evident in Tables 3 and 4.

The average crystallite sizes of the Series II samples depicted in Table 5 were obtained through the Scherrer equation, utilizing an analysis of the diffraction peaks of Figure 6 with the X'Pert HighScore Plus software.

Box 10

Table 5

Crystallite Size Analysis of Series II Samples

Sample	Crystallite size [Å]
II-1	98.8
II-1	84.5
II-1	650.5

Source: own elaboration

Figure 6 presents the diffractograms corresponding to the various samples from Series II. Notably, when the precursor solution employed a 1:1 ratio of HNO_3 to HCl (sample II-3), titanium oxide oxalate hydroxide hydrate was obtained, consistent with the crystallographic data from ICDD 00-048-1164.

In contrast, for other ratios, only the rutile phase was identified, as indicated by the crystallographic card ICDD 01-073-1765.

Box 11
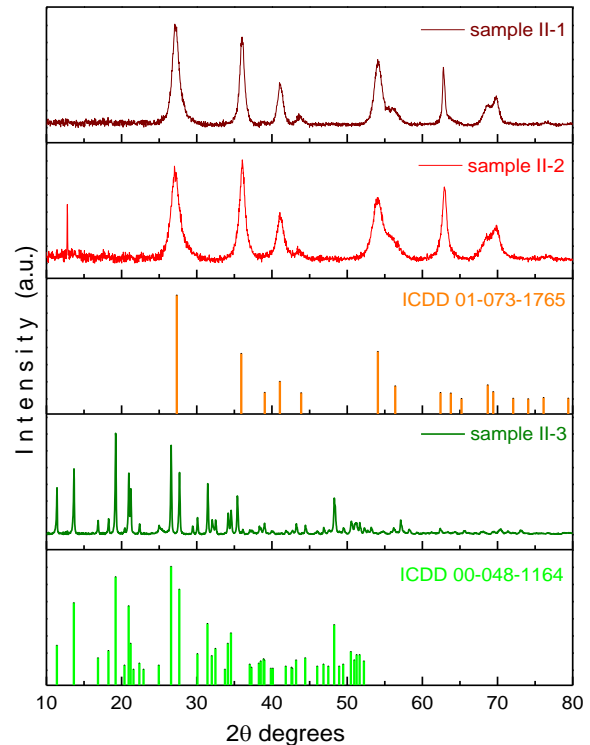
Figure 6

X-ray diffraction patterns of Series II

Source: Own elaboration

Characterization by ATR-FTIR

The functional groups present in the samples were identified by ATR-FTIR spectroscopy.

The FTIR transmission spectrum of Series I samples, calcined at 300°C and 500°C, is shown in Figure 7. Notably, the spectrum reveals the presence of broad bands associated with hydroxyl groups (O–H stretching vibration) in the 3000 cm^{-1} – 3600 cm^{-1} range. Specifically, for sample I-1, synthesized without HNO_3, the corresponding peak related to this OH group is notably small.

Additionally, a band around 1650 cm^{-1} is attributed to absorbed water molecules (H–O–H symmetric vibration) on the surface of the TiO_2 crystal (Sanchez-Martinez, 2019). Furthermore, the broad band spanning the 1000 cm^{-1} to 400 cm^{-1} region is ascribed to Ti-O stretching and Ti-O-Ti bridging stretching modes (Praveen, 2014).

Box 12
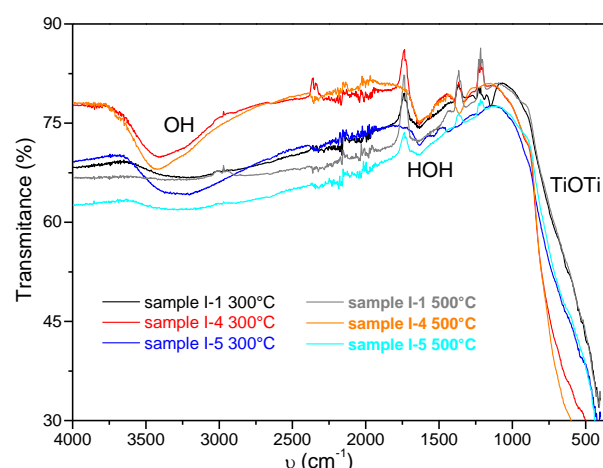
Figure 7

ATR-FTIR spectra of Series I samples

Source: Own elaboration

      The ATR-FTIR spectra of Series II samples, observed on Figure 8, exhibit several distinct absorption bands that can be attributed to the various vibrational modes of the oxalate and titanium-oxygen bonding. For instance, the band in the 3000 cm^{-1} – 3600 cm^{-1} range is associated with hydroxyl groups (O–H stretching vibration) (Sanchez-Martinez, 2019), a band in the region of 2300-2400 cm^{-1} is frequently observed and is attributed to the adsorption of atmospheric CO_2 on the sample surface during the measurement (Liu, 2014), the strong absorption bands observed in the 1600-1700 cm^{-1} region on sample II-3 are characteristic of the C=O stretching vibrations of the oxalate group (Young, 2009) while to samples II-1 and II-2 this band is associated with the NO-stretching (Nishikiori, 2011), the band at around 900 cm^{-1} is associated to the Ti-O-Ti vibrations (Haggerty et al., 2017) and the band that appears around 800 cm^{-1} range are associated with the Ti-O stretching vibrations (Liu, 2014).

Box 13
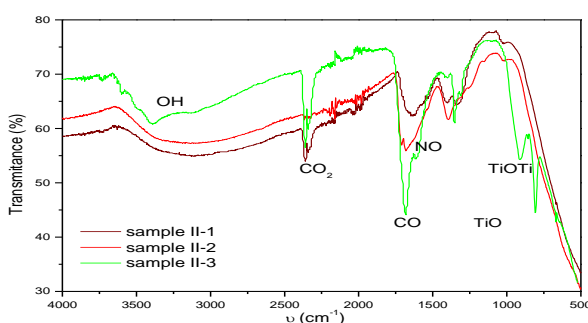
Figure 8

ATR-FTIR spectra of Series II samples

Source: own elaboration

Characterization by SEM

Scanning Electron Microscopy (SEM) images provides detailed insights into the morphology and structure of materials. In Series I, Figures 9 to 18 display a scale bar on the left side, indicating 1 micron, emphasizing the high magnification level. On the right side, these figures zoom in further, revealing finer details with a 20 nm scale bar. For Series II, Figures 19 to 21 show a scale bar on the upper side, also indicating 1 micron, highlighting the high magnification level. The lower side of these figures provides even closer views, displaying finer details with a 200 or 100 nm scale bar.

Box 14
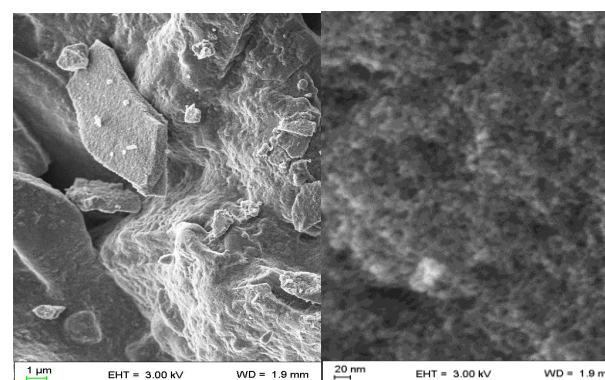
Figure 9

SEM micrograph of Sample I-1 calcinated at 300ºC
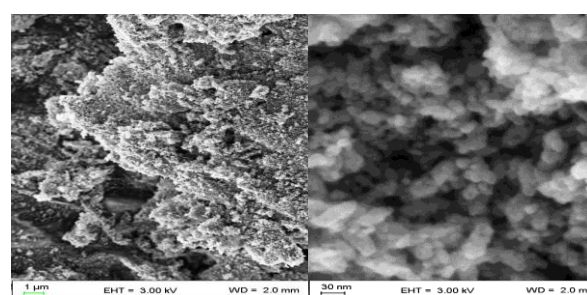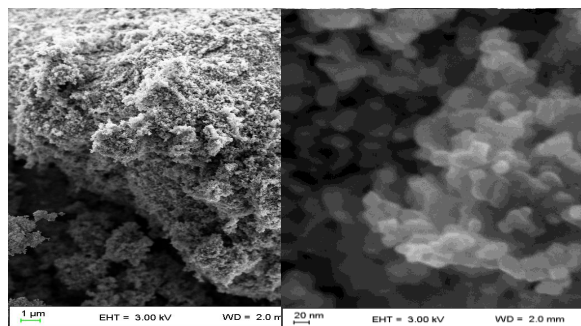
Source: Carl Zeiss Supra 40

Box 15
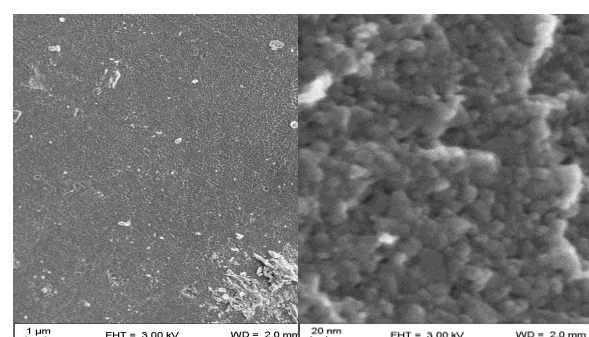
Figure 10

Sample I-1 calcinated at 500ºC

Source: Carl Zeiss Supra 40

      Figure 9 shows the morphology of sample I-1 calcinated at 300°C. At this temperature, various structures are visible, including flat, angular plate-like formations and fibrous patterns on surface texture, the particle size appears to be in the nanometer range, and there is minimal evidence of agglomeration. The overall structure is porous, which is typical for TiO2 calcinated at lower temperatures.

In contrast, the SEM image in Figure 10 of the sample calcinated at 500°C shows that particles are larger and more crystalline compared to those in Figures 9, there is a noticeable increase in particle size, and the surface texture appears relatively smooth, with occasional roughness. Additionally, there is evidence of particle sintering, leading to a denser structure with reduced porosity.

Box 16
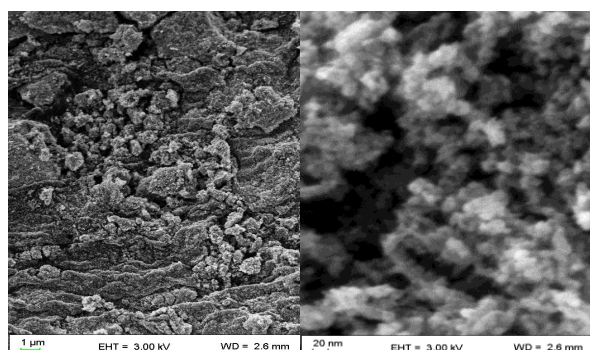
Figure 11

Sample I-2 calcinated at 300°C

Source: Carl Zeiss Supra 40

Box 17
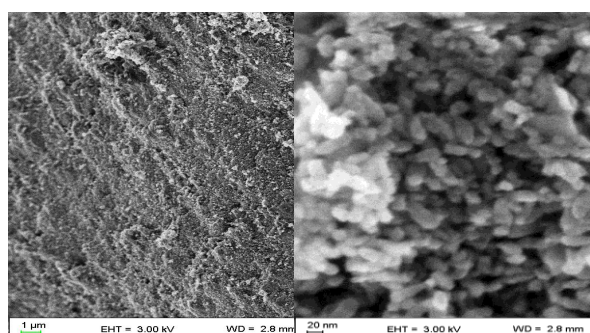
Figure 12

Sample I-2 calcinated at 500°C
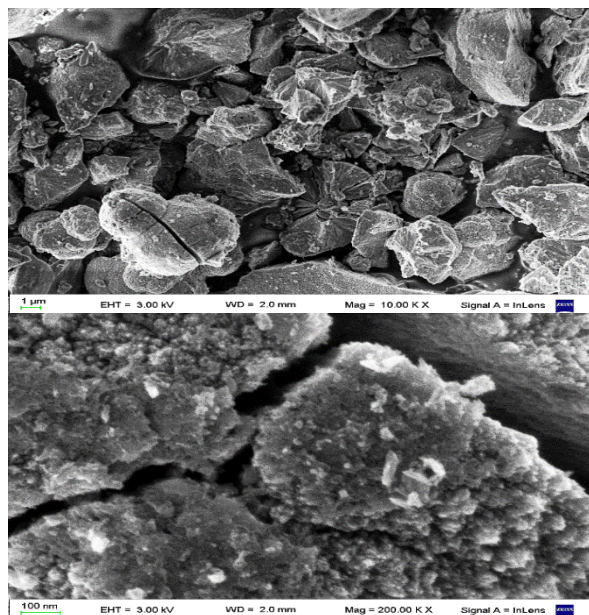
Source: Carl Zeiss Supra 40

The SEM image of sample I-2 calcinated at 300°C shown on Figure 11, appears more irregular and porous compared to the same sample calcined at 500°C (Figure 12) which exhibits a more uniform and crystalline structure.

This suggests that higher calcination temperature have improved the crystallinity and reduced the surface defects of the nanoparticles, the differences in morphology are attributed to the increased thermal energy promoting the elimination of surface defects, leading to a more ordered and crystalline structure.

Box 18
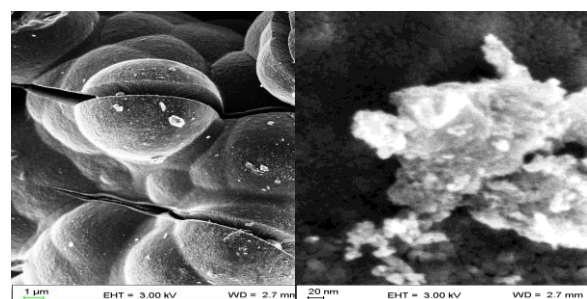
Figure 13

Sample I-3 calcinated at 300°C

Source: Carl Zeiss Supra 40

Box 19
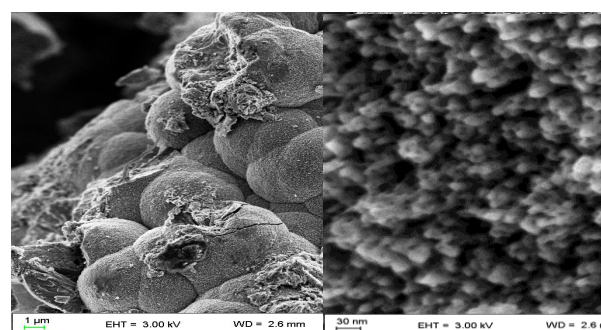
Figure 14

Sample I-3 calcinated at 500°C

Source: Carl Zeiss Supra 40

For sample I-3, Figure 13, calcinated at 300°C exhibiting a more porous and fibrous structure compared to Figure 14 related to the sample calcinated at 500°C, which displayed a denser and more crystalline appearance. This change in morphology was attributed to the increased thermal energy imparted to the TiO_2 particles during the higher temperature calcination process. The higher thermal energy input also affected the particle size distribution, with the 500°C calcined sample displaying a narrower and more finely dispersed particle size distribution compared to the 300°C calcined sample.

Box 20

Figure 15

Sample I-4 calcinated at 300°C

Source: Carl Zeiss Supra 40

Del Ángel-Sánchez, María Magdalena & Martínez-Carreón, María de Jesús. [2024]. Influence of concentration, acid type and calcination temperature on TiO₂ synthesis. Journal of Systematic Innovation. 8[22]1-11: e4822111.
https://doi.org/10.35429/JSI.2024.8.22.1.11

Box 21

Figure 16

Sample I-4 calcinated at 500ºC

Source: Carl Zeiss Supra 40

SEM micrograph of sample I-4 calcinated at 300°C are displayed on Figure 15 and Figure 16 corresponds to the same sample calcinated at 500°C. It is observed that the micrographs show change in crystal structure and surface morphology after calcination at 500°C compared to 300°C. The surface morphology of image calcinated at 300°cindicates a relatively rough and porous nature with irregularly shaped particles, whereas the surface morphology of image calcinated at 500°C exhibits a much smoother and more uniform surface with smaller and more rounded particles.

Box 22
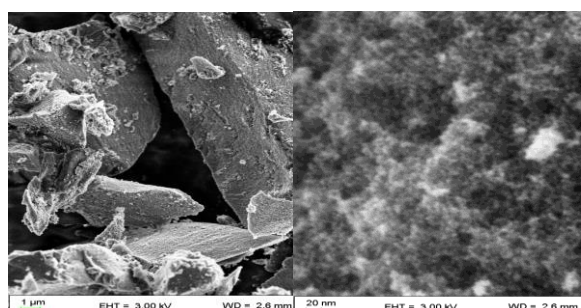
Figure 17

Sample I-5 calcinated at 300ºC

Source: Carl Zeiss Supra 40

Box 23
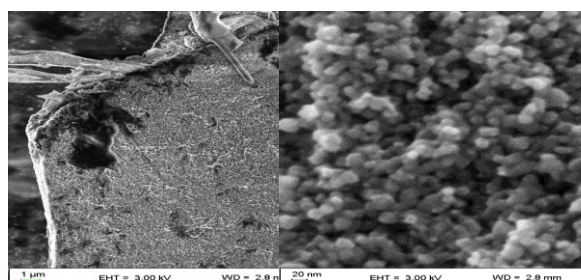
Figure 18

Sample I-5 calcinated at 500ºC

Source: Carl Zeiss Supra 40

The differences observed in the SEM images of sample I-5 can be attributed to the impact of calcination temperature on the crystallization and phase transformation. The lower calcination temperature of 300°C was not sufficient to fully promote the crystallization of TiO_2, leading to the formation of larger, more irregular, and fibrous particles like is observed on Figure 17, this is likely due to the incomplete phase transformation from the amorphous to the crystalline phase. In contrast, Figure 18 indicates that the higher calcination temperature of 500°C enabled the complete crystallization of the material. This resulted in the formation of smaller, more uniform, and spherical particles with a relatively smooth surface morphology. The elevated temperature facilitated improved atomic rearrangement and the growth of well-defined titania crystal structures.

SEM images in Figures 19 to 21 depict the titania synthesis process using varying ratios of nitric acid (HNO_3) to hydrochloric acid (HCl).

Box 24
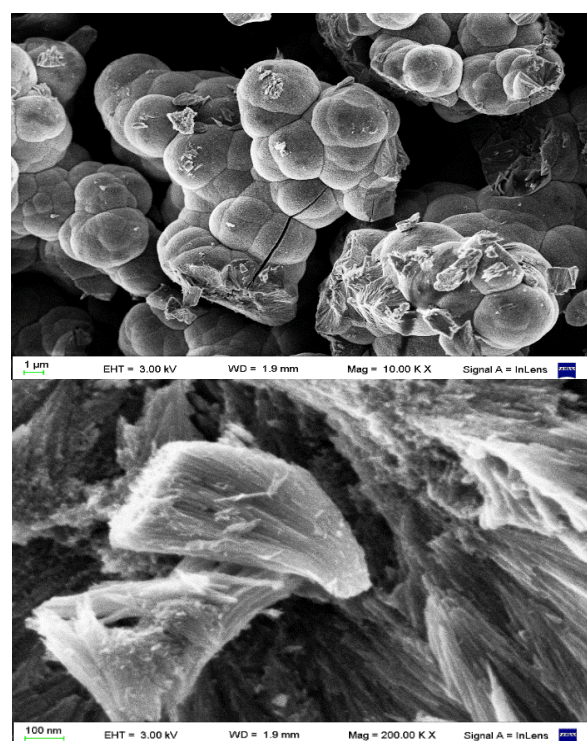
Figure 19

Sample II-1, obtained with a 1:5 ratio of HNO_3 to HCl

Source: Carl Zeiss Supra 40

Box 25

Figure 20

Sample II-2, obtained with a 1:2 ratio of HNO₃ to HCl

Source: Carl Zeiss Supra 40

Figure 19 corresponds to the product obtained with a 1:5 HNO₃-to-HCl ratio, Figure 20 with a 1:2 ratio, and Figure 21 with a 1:1 ratio. Figures 19 and 20 indeed reveal similar particle morphology, characterized by spherical shapes. The confirmation through X-ray diffraction (XRD) analysis further supports the presence of the rutile phase of titanium dioxide in these samples.

Box 26
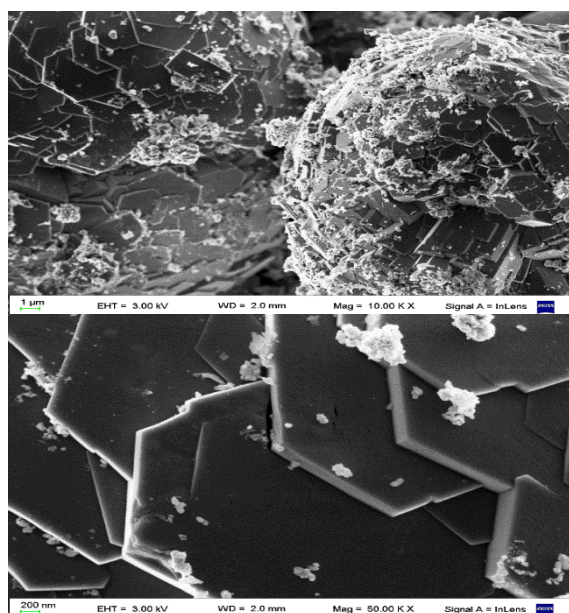
Figure 21

Sample II-3, obtained with a 1:1 ratio of HNO₃ to HCl

Source: Carl Zeiss Supra 40

However, Figure 21 represents a distinct scenario, the synthesis of titanium oxalate. The particles in this case exhibit hexagonal shapes, indicating a different crystal structure and morphology compared to the rutile phase observed in figures 19 and 20.

The impact of the HNO₃-to-HCl ratio on the final product on the crystalline phase has significantly influences. In the case of rutile, the 1:5 and 1:2 ratios (Figures 19 and 20) favor its formation. However, the 1:1 ratio (Figure 21) leads to the synthesis of titanium oxalate. The specific acid concentrations affect the availability of precursor ions and their interactions during nucleation and growth When considering particle size and shape, smaller acid ratios may promote nucleation and result in smaller particles, while larger ratios may lead to larger particles. The spherical morphology observed in rutile (Figures 19 and 20) suggests controlled growth under specific conditions. The hexagonal shapes in titanium oxalate (Figure 21) indicate different growth mechanisms. Beyond individual particles, the overall morphology of the synthesized material is influenced. The arrangement of particles, agglomeration, and surface features contribute to the macroscopic appearance. The distinct hexagonal coverage in Figure 21 highlights the unique morphology of titanium oxalate.

Conclusions

In Series 1, it was observed that higher nitric acid concentrations predominantly favor the development of the rutile phase, while lower concentrations lead to the formation of the anatase phase. Intermediate acid concentrations result in more stable sols. Furthermore, the pronounced aggregation and rougher surface of the particles calcined at 300°C suggest that the lower calcination temperature was not sufficient to overcome the attractive forces between the particles, leading to the formation of larger agglomerates. In comparison, the higher temperature of 500°C enabled better control over the particle growth, resulting in a more uniform and less aggregated particle distribution. Notably, the type and concentration of acid exert a more significant influence on phase determination than thermal treatment. Additionally, the presence of fluoride induces a slight increase in nanoparticle size.

In Series 2, it was determined that a higher proportion of hydrochloric acid (HCl) compared to nitric acid (HNO₃) induces the formation of the rutile phase of TiO₂. Conversely, when the acid ratio is equal, that is, a 1:1 proportion, the generation of Titanium oxide oxalate hydroxide hydrate is favored.

These findings underscore the significance of acid composition in hydrothermal synthesis and its direct influence on the crystalline phase, particle size and shape and overall morphology of the synthesized titanium-based materials.

Declarations

Conflict of interest

The authors hereby declare that there are no conflicts of interest associated with this publication

Authors' Contributions

All authors have made equal and significant contributions to the development and completion of this research paper. Each author has been actively involved in the conceptualization, experimental analysis, and interpretation of the research findings.

Availability of data and materials

All data generated or analyzed during this study are included in this published manuscript

Financing

Acknowledgements

Abbreviations

ATR-FTIR	Attenuated Total Reflectance Fourier Transform Infrared Spectroscopy
DLS	Dynamic Light Scattering
FESEM	Field Emission Scanning Electron Data Microscopy
HCl	Hydrochloric acid
HNO₃	Nitric acid
ICDD	The International Centre for Diffraction
MOCVD	X-Ray Diffraction
NaF	metal-organic chemical vapor deposition
SEM	Sodium fluoride
Ti i(PrO)₄	Scanning Electron Microscopy
TiO₂	Titanium isopropoxide
XRD	Titanium Dioxide
	X-ray diffraction

References

Background

Ali, I., Suhail, M., Alothman, Z. A., & Alwarthan, A. (2018). Recent advances in syntheses, properties and applications of TiO2 nanostructures. RSC Advances, 8(53), 30125–30147.

Background

Anandgaonker, P., Kulkarni, G., Gaikwad, S., & Rajbhoj, A. (2019). Synthesis of TiO2 nanoparticles by electrochemical method and their antibacterial application. Arabian Journal of Chemistry, 12(8), 1815–1822.

Arun, J., Nachiappan, S., Rangarajan, G., Alagappan, R. P., Gopinath, K. P., & Lichtfouse, E. (2023). Synthesis and application of titanium dioxide photocatalysis for energy, decontamination and viral disinfection: a review. Environmental Chemistry Letters, 21(1), 339–362.

Dülger, B., Özkan, G., Angı, O. S., & Özkan, G. (2024). Green synthesis of TiO2 nanoparticles using Aloe Vera extract as catalyst support material and studies of their catalytic activity in dehydrogenation of Ethylenediamine Bisborane. International Journal of Hydrogen Energy.

Farooq, N., Kallem, P., ur Rehman, Z., Imran Khan, M., Kumar Gupta, R., Tahseen, T., Mushtaq, Z., Ejaz, N., & Shanableh, A. (2024). Recent trends of titania (TiO₂) based materials: A review on synthetic approaches and potential applications. Journal of King Saud University. Science, 36(6), 103210.

Guo, J., Zhu, S., Chen, Z., Li, Y., Yu, Z., Liu, Q., Li, J., Feng, C., & Zhang, D. (2011). Sonochemical synthesis of TiO2 nanoparticles on graphene for use as photocatalyst. Ultrasonics Sonochemistry, 18(5), 1082–1090.

Hidalgo, M. C., Aguilar, M., Maicu, M., Navío, J. A., & Colón, G. (2007). Hydrothermal preparation of highly photoactive TiO2 nanoparticles. Catalysis Today, 129(1–2), 50–58.

Li, W., Ismat Shah, S., Huang, C.-P., Jung, O., & Ni, C. (2002). Metallorganic chemical vapor deposition and characterization of TiO2 nanoparticles. Materials Science & Engineering. B, Solid-State Materials for Advanced Technology, 96(3), 247–253.

Pelaez, M., Nolan, N. T., Pillai, S. C., Seery, M. K., Falaras, P., Kontos, A. G., Dunlop, P. S. M., Hamilton, J. W. J., Byrne, J. A., O'Shea, K., Entezari, M. H., & Dionysiou, D. D. (2012). A review on the visible light active titanium dioxide photocatalysts for environmental applications. Applied Catalysis. B, Environmental, 125, 331–349.

Basics

Bindra, P., Mittal, H., Sarkar, B. R., & Hazra, A. (2022). Synthesis of highly ordered TiO2 nanorods on a titanium substrate using an optimized hydrothermal method. Journal of Electronic Materials, 51(4), 1707–1716.

Eaimsumang, S., Prataksanon, P., Pongstabodee, S., & Luengnaruemitchai, A. (2020). Effect of acid on the crystalline phase of TiO2 prepared by hydrothermal treatment and its application in the oxidative steam reforming of methanol. Research on Chemical Intermediates, 46(2), 1235–1254.

Gupta, T., Samriti, Cho, J., & Prakash, J. (2021). Hydrothermal synthesis of TiO2 nanorods: formation chemistry, growth mechanism, and tailoring of surface properties for photocatalytic activities. Materials Today. Chemistry, 20(100428), 100428.

Kignelman, G., & Thielemans, W. (2021). Meta-analysis of TiO2 nanoparticle synthesis strategies to assess the impact of key reaction parameters on their crystallinity. Journal of Materials Science, 56(10), 5975–5994.

Rehan, M., Lai, X., & Kale, G. M. (2011). Hydrothermal synthesis of titanium dioxide nanoparticles studied employing in situ energy dispersive X-ray diffraction. CrystEngComm, 13(11), 3725.

Support

Haggerty, J. E. S., Schelhas, L. T., Kitchaev, D. A., Mangum, J. S., Garten, L. M., Sun, W., Stone, K. H., Perkins, J. D., Toney, M. F., Ceder, G., Ginley, D. S., Gorman, B. P., & Tate, J. (2017). High-fraction brookite films from amorphous precursors. Scientific Reports, 7(1), 1–11.

Liu, C., Zhang, D., & Sun, Y. (2014). Synthesis of hollow anatase spheres with enhanced optical performance. CrystEngComm, 16(36), 8421.

Nishikiori, H., Fukasawa, Y., Yokosuka, Y., & Fujii, T. (2011). Nitrogen doping into titanium dioxide by the sol–gel method using nitric acid. Research on Chemical Intermediates, 37(8), 869–881.

Sanchez-Martinez, A., Koop-Santa, C., Ceballos-Sanchez, O., López-Mena, E. R., González, M. A., Rangel-Cobián, V., Orozco-Guareño, E., & García-Guaderrama, M. (2019). Study of the preparation of TiO2 powder by different synthesis methods. Materials Research Express, 6(8), 085085.

Praveen, P., Viruthagiri, G., Mugundan, S., & Shanmugam, N. (2014). Structural, optical and morphological analyses of pristine titanium di-oxide nanoparticles – Synthesized via sol–gel route. Spectrochimica Acta. Part A, Molecular and Biomolecular Spectroscopy, 117, 622-629.

Instructions for Scientific, Technological and Innovation Publication

[[Title in TNRoman and Bold No. 14 in English and Spanish]

Surname, Name 1st Author*a, Surname, Name 1st Co-authorb, Surname, Name 2nd Co-authorc and Surname, Name 3rd Co-authord [No.12 TNRoman]

a ROR [Affiliation institution](), ⟳ [Researcher ID](), ⓘD [ORC ID](), [SNI-CONAHCYT ID]() or CVU PNPC [No.10 TNRoman]
b ROR Affiliation institution, ⟳ Researcher ID, ⓘD ORC ID, SNI-CONAHCYT ID or CVU PNPC [No.10 TNRoman]
c ROR Affiliation institution, ⟳ Researcher ID, ⓘD ORC ID, SNI-CONAHCYT ID or CVU PNPC [No.10 TNRoman]
d ROR Affiliation institution, ⟳ Researcher ID, ⓘD ORC ID, SNI-CONAHCYT ID or CVU PNPC [No.10 TNRoman]

All ROR-Clarivate-ORCID and CONAHCYT profiles must be hyperlinked to your website.
Prot- ROR [University of South Australia]() • ⟳ [7038-2013]()• ⓘD [0000-0001-6442-4409]() • ⊕ 416112

Abstract [In English]
Must contain up to 150 words
Graphical abstract [In English]

Your title goes here		
Objectives	Methodology	Contribution

Authors must provide an original image that clearly represents the article described in the article. Graphical abstracts should be submitted as a separate file. Please note that, as well as each article must be unique. File type: the file types are MS Office files.No additional text, outline or synopsis should be included. Any text or captions must be part of the image file. Do not use unnecessary white space or a "graphic abstract" header within the image file.

Keywords [In English]
Indicate 3 keywords in TNRoman and Bold No. 10

Abstract [In Spanish]
Must contain up to 150 words
Graphical abstract [In Spanish]

Your title goes here		
Objectives	Methodology	Contribution

Authors must provide an original image that clearly represents the article described in the article. Graphical abstracts should be submitted as a separate file. Please note that, as well as each article must be unique. File type: the file types are MS Office files.No additional text, outline or synopsis should be included. Any text or captions must be part of the image file. Do not use unnecessary white space or a "graphic abstract" header within the image file.

Keywords [In Spanish]
Indicate 3 keywords in TNRoman and Bold No. 10

Instructions for Scientific, Technological and Innovation Publication

Introduction

Text in TNRoman No.12, single space.

General explanation of the subject and explain why it is important.

What is your added value with respect to other techniques?

Clearly focus each of its features.

Clearly explain the problem to be solved and the central hypothesis.

Explanation of sections Article.

Development of headings and subheadings of the article with subsequent numbers

[Title No.12 in TNRoman, single spaced and bold]

Products in development No.12 TNRoman, single spaced.

Including figures and tables-Editable

In the article content any table and figure should be editable formats that can change size, type and number of letter, for the purposes of edition, these must be high quality, not pixelated and should be noticeable even reducing image scale.

[Indicating the title at the bottom with No.10 and Times New Roman Bold]

Box
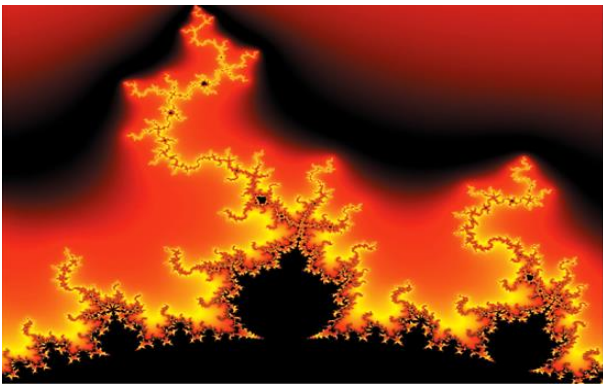
Figure 1

Title [Should not be images-everything must be editable]
Source [in italic]

Box

Table 1

Title [Should not be images-everything must be editable]

Source [in italic]

The maximum number of Boxes is 10 items

For the use of equations, noted as follows:

$$Y_{ij} = \alpha + \sum_{h=1}^{r} \beta_h X_{hij} + u_j + e_{ij} \qquad [1]$$

Must be editable and number aligned on the right side.

Methodology

Develop give the meaning of the variables in linear writing and important is the comparison of the used criteria.

Results

The results shall be by section of the article.

Conclusions

Clearly explain the results and possibilities of improvement.

Annexes

Tables and adequate sources.
The international standard is 7 pages minimum and 14 pages maximum.
Declarations

Conflict of interest

The authors declare no interest conflict. They have no known competing financial interests or personal relationships that could have appeared to influence the article reported in this article.

Surname (IN UPPERCASE), Name 1st Author, Surname (IN UPPERCASE), Name 1st Co-author, Surname (IN UPPERCASE), Name 2nd Co-author and Surname (IN UPPERCASE), Name 3rd Co-author. Paper Title ECORFAN Journal- Taiwan. Year [Times New Roman No. 8]

Instructions for Scientific, Technological and Innovation Publication

Author contribution

Specify the contribution of each researcher in each of the points developed in this research.

Prot-
Benoit-Pauleter, Gerard: Contributed to the project idea, research method and technique.

Availability of data and materials

Indicate the availability of the data obtained in this research.

Funding

Indicate if the research received some financing.

Acknowledgements

Indicate if they were financed by any institution, University or company.

Abbreviations

List abbreviations in alphabetical order.

Prot-
ANN   Artificial Neural Network

References

Use APA system. Should not be numbered, nor with bullets, however if necessary numbering will be because reference or mention is made somewhere in the Article.

Use the Roman alphabet, all references you have used should be in Roman alphabet, even if you have cited an article, book in any of the official languages of the United Nations [English, French, German, Chinese, Russian, Portuguese, Italian, Spanish, Arabic], you should write the reference in Roman alphabet and not in any of the official languages.

Citations are classified the following categories:

Antecedents. The citation is due to previously published research and orients the citing document within a particular scholarly area.

Basics. The citation is intended to report data sets, methods, concepts and ideas on which the authors of the citing document base their work.

Supports. The citing article reports similar results. It may also refer to similarities in methodology or, in some cases, to the reproduction of results.

Differences. The citing document reports by means of a citation that it has obtained different results to those obtained in the cited document. This may also refer to differences in methodology or differences in sample sizes that affect the results.

Discussions. The citing article cites another study because it is providing a more detailed discussion of the subject matter.

The URL of the resource is activated in the DOI or in the title of the resource.

Prot-
Mandelbrot, B. B. [2020]. Negative dimensions and Hölders, multifractals and their Hölder spectra, and the role of lateral preasymptotics in science. Journal of Fourier Analysis and Applications Special. 409-432.

Intellectual Property Requirements for editing:

- Authentic Signature in Color of Originality Format Author and Coauthors.

- Authentic Signature in Color of the Acceptance Format of Author and Coauthors.

- Authentic Signature in blue color of the Conflict of Interest Format of Author and Co-authors.

Reservation to Editorial Policy

Journal of Systematic Innovation reserves the right to make editorial changes required to adapt the Articles to the Editorial Policy of the Journal. Once the Article is accepted in its final version, the Research Journal will send the author the proofs for review. ECORFAN® will only accept the correction of errata and errors or omissions arising from the editing process of the Journal, reserving in full the copyrights and content dissemination. No deletions, substitutions or additions that alter the formation of the Article will be accepted.

Code of Ethics - Good Practices and Declaration of Solution to Editorial Conflicts

Declaration of Originality and unpublished character of the Article, of Authors, on the obtaining of data and interpretation of results, Acknowledgments, Conflict of interests, Assignment of rights and Distribution

The ECORFAN-Mexico, S.C Management claims to Authors of Articles that its content must be original, unpublished and of Scientific, Technological and Innovation content to be submitted for evaluation.

The Authors signing the Article must be the same that have contributed to its conception, realization and development, as well as obtaining the data, interpreting the results, drafting and reviewing it. The Corresponding Author of the proposed Article will request the form that follows.

Article title:

- – The sending of an Article to Journal of Systematic Innovation emanates the commitment of the author not to submit it simultaneously to the consideration of other series publications for it must complement the Format of Originality for its Article, unless it is rejected by the Arbitration Committee, it may be withdrawn.

- – None of the data presented in this article has been plagiarized or invented. The original data are clearly distinguished from those already published. And it is known of the test in PLAGSCAN if a level of plagiarism is detected Positive will not proceed to arbitrate.

- – References are cited on which the information contained in the Article is based, as well as theories and data from other previously published Articles.

- – The authors sign the Format of Authorization for their Article to be disseminated by means that ECORFAN-Mexico, S.C. In its Holding Taiwan considers pertinent for disclosure and diffusion of its Article its Rights of Work.

- – Consent has been obtained from those who have contributed unpublished data obtained through verbal or written communication, and such communication and Authorship are adequately identified.

- – The Author and Co-Authors who sign this work have participated in its planning, design and execution, as well as in the interpretation of the results. They also critically reviewed the paper, approved its final version and agreed with its publication.

- – No signature responsible for the work has been omitted and the criteria of Scientific Authorization are satisfied.

- – The results of this Article have been interpreted objectively. Any results contrary to the point of view of those who sign are exposed and discussed in the Article.

Copyright and Access

Article Title:

Name and Surnames of the Contact Author and the Coauthors	Signature
1.	
2.	
3.	
4.	

Principles of Ethics and Declaration of Solution to Editorial Conflicts

Editor Responsibilities

The Publisher undertakes to guarantee the confidentiality of the evaluation process, it may not disclose to the Arbitrators the identity of the Authors, nor may it reveal the identity of the Arbitrators at any time.

The Editor assumes the responsibility to properly inform the Author of the stage of the editorial process in which the text is sent, as well as the resolutions of Double-Blind Review.

The Editor should evaluate manuscripts and their intellectual content without distinction of race, gender, sexual orientation, religious beliefs, ethnicity, nationality, or the political philosophy of the Authors.

The Editor and his editing team of ECORFAN® Holdings will not disclose any information about Articles submitted to anyone other than the corresponding Author.

The Editor should make fair and impartial decisions and ensure a fair Double-Blind Review.

Responsibilities of the Editorial Board

The description of the peer review processes is made known by the Editorial Board in order that the Authors know what the evaluation criteria are and will always be willing to justify any controversy in the evaluation process. In case of Plagiarism Detection to the Article the Committee notifies the Authors for Violation to the Right of Scientific, Technological and Innovation Authorization.

Responsibilities of the Arbitration Committee

The Arbitrators undertake to notify about any unethical conduct by the Authors and to indicate all the information that may be reason to reject the publication of the Articles. In addition, they must undertake to keep confidential information related to the Articles they evaluate.

Any manuscript received for your arbitration must be treated as confidential, should not be displayed or discussed with other experts, except with the permission of the Editor.

The Arbitrators must be conducted objectively, any personal criticism of the Author is inappropriate.

The Arbitrators must express their points of view with clarity and with valid arguments that contribute to the Scientific, Technological and Innovation of the Author.

The Arbitrators should not evaluate manuscripts in which they have conflicts of interest and have been notified to the Editor before submitting the Article for Double-Blind Review.

Responsibilities of the Authors

Authors must guarantee that their articles are the product of their original work and that the data has been obtained ethically.

Authors must ensure that they have not been previously published or that they are not considered in another serial publication.

Authors must strictly follow the rules for the publication of Defined Articles by the Editorial Board.

The authors have requested that the text in all its forms be an unethical editorial behavior and is unacceptable, consequently, any manuscript that incurs in plagiarism is eliminated and not considered for publication.

Authors should cite publications that have been influential in the nature of the Article submitted to arbitration.

Information services

Indexation - Bases and Repositories

RESEARCH GATE (Germany)
GOOGLE SCHOLAR (Citation indices-Google)
MENDELEY (Bibliographic References Manager)
REDIB (Ibero-American Network of Innovation and Scientific Knowledge- CSIC)
HISPANA (Information and Bibliographic Orientation-Spain)

Publishing Services

Citation and Index Identification H
Management of Originality Format and Authorization
Testing Article with PLAGSCAN
Article Evaluation
Certificate of Double-Blind Review
Article Edition
Web layout
Indexing and Repository
ArticleTranslation
Article Publication
Certificate of Article
Service Billing

Editorial Policy and Management

69 Street. YongHe district, ZhongXin. Taipei-Taiwan. Phones: +52 1 55 6159 2296, +52 1 55 1260 0355, +52 1 55 6034 9181; Email: contact@ecorfan.org www.ecorfan.org

Journal of Systematic Innovation